# The low-$Q^2$, low-$x$ region in electroproduction

B. Badełek

*Department of Physics, Uppsala University, P.O. Box 530, 751 21 Uppsala, Sweden and Institute of Experimental Physics, Warsaw University, Hoża 69, 00-681 Warsaw, Poland*

J. Kwieciński

*H. Niewodniczański Institute of Nuclear Physics, Radzikowskiego 152, 31-342 Cracow, Poland*

The authors summarize existing experimental and theoretical knowledge of the structure function $F_2$ in the region of low $Q^2$ and low $x$. Constraints on the behavior of structure functions in the limit of $Q^2=0$ are listed. Phenomenological low-$Q^2$ parametrizations of $F_2$ are collected, and their dynamical content is discussed. High-energy photoproduction and nuclear shadowing are described briefly. A recent update of the low-$Q^2$, low-$x$ experimental data and their implications is given.

## CONTENTS

I. Introduction 445
II. Basic Definitions and Constrains 446
III. Basic Theoretical Concepts Relevant to the Small $Q^2$ Region 447
IV. High-Energy Photoproduction 448
V. Phenomenological Parametrizations of Structure Functions 450
VI. Dynamical Models of the Low-$Q^2$ Behavior of $F_2$ 454
VII. Nuclear Shadowing 461
VIII. Experimental Data 466
IX. Conclusions and Outlook 469
Acknowledgments 469
References 470

## I. INTRODUCTION

Inelastic electron (muon)-nucleon scattering, known as electroproduction, is an abundant source of information about nucleon structure. The kind of information obtainable from experiments depends on $Q^2$, the negative of the square of the four-momentum transferred by the lepton to the nucleon. In the region of high $Q^2$ the results of electroproduction measurements are interpreted in terms of partons (quarks and gluons). The theoretical framework is provided in this case by the QCD-improved parton model. This description fails when $Q^2$ becomes of the order of 1 GeV$^2$, and a different dynamical picture emerges which is still not fully understood.

Present fixed-target experiments operating in the region of low $Q^2$ measure electroproduction for low values of the Bjorken variable $x$ as well (see, for example, Amaudruz *et al.*, 1992b, 1992c). This fact justifies interest in low-$Q^2$, low-$x$ phenomena in elastic lepton-hadron scattering. The breakdown of the parton picture recently appeared in a new context, in measurements carried out at both high and low $Q^2$ and small $x$ at the HERA collider. It now seems that understanding the transition from high- to low-$Q^2$ dynamics in the low-$x$ region is one of the most challenging problems of the day. A unified treatment of the small- and large-$Q^2$ regions might also be of great practical importance for large-$Q^2$ data analysis. This is because in all leptoproduction experiments, including those at HERA, a radiative-corrections procedure must be applied in order to extract the structure functions from the data. The radiative ''tails'' originating from processes at $Q^2$ in the interval $Q^2_{\rm meas}\geqslant Q^2\geqslant 0$ contribute to measurements at $Q^2=Q^2_{\rm meas}$, and knowledge of the structure functions in this $Q^2$ interval is necessary for the iterative data-unfolding procedure (Badełek, Bentvelsen, Kooijman, Kwieciński, Spiesberger, and von Schlippe, 1993; Badełek, Bardin, Kurek, and Scholz, 1995).

The inelastic electron-nucleon cross section is described by two structure functions, $F_1(x,Q^2)$ and $F_2(x,Q^2)$. Remembering that due to conservation of the electromagnetic current the structure function $F_2$ must vanish in the limit $Q^2\to 0$, the Bjorken scaling which holds approximately at high $Q^2$ cannot be valid at low $Q^2$. Theoretical models assuring a smooth transition from the scaling to the nonscaling region and applicable in a wide $Q^2$ interval are thus necessary for understanding the experimental data and the underlying dynamics. The continuity of the physical processes occurring when passing from low to high $Q^2$ is illustrated in Fig. 1. We shall be concerned predominantly with the region of low $Q^2$ and high $W$, i.e., beyond the resonances ($W$ is the invariant mass of the electroproduced hadron system).

The need to modify the QCD-improved parton model by including contributions to the structure functions behaving as $1/(Q^2)^n (n\geqslant 1)$ is clearly visible in the data [Arneodo *et al.* (NMC), 1993]. These contributions, called ''higher twists,'' are important at moderate values of $Q^2(\sim 1$ GeV$^2)$. They follow from the operator-product expansion (Roberts, 1990) and describe effects of the struck parton's interaction with target remnants, thus reflecting confinement effects. Clearly, a theoretical description unifying the confinement and deep-inelastic regions should contain terms of well-defined physical origin corresponding to such contributions.

The main purpose of this paper is to collect existing knowledge about the region of low $Q^2$, low $x$ (i.e., $Q^2$ below 3 GeV$^2$ and $x$ below 0.03 or so) in such a way that it is easy to use in practical applications. The paper

  

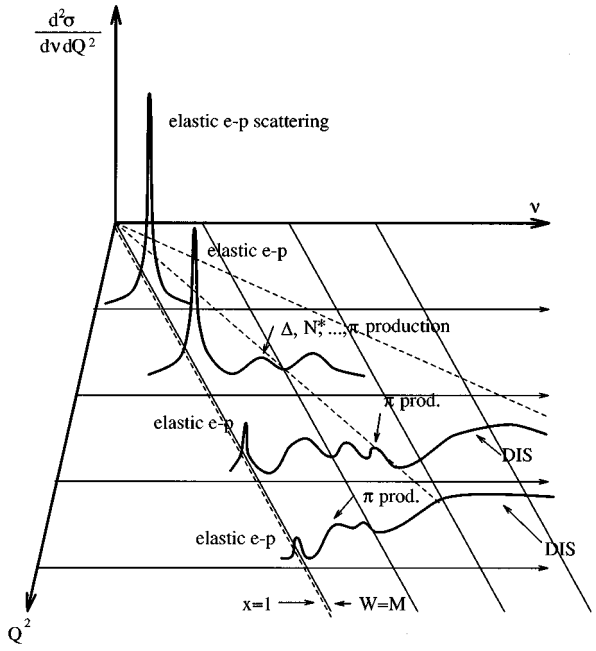


FIG. 1. Illustration of the continuity of physical processes: the double differential cross section for electron-proton inelastic scattering is sketched as a function of the energy transfer $\nu$ for different values of the resolution $Q^2$. Dashed and continuous lines correspond to constant values of $x$ and $W$, respectively. Definitions of kinematic variables are given in Sec. II.

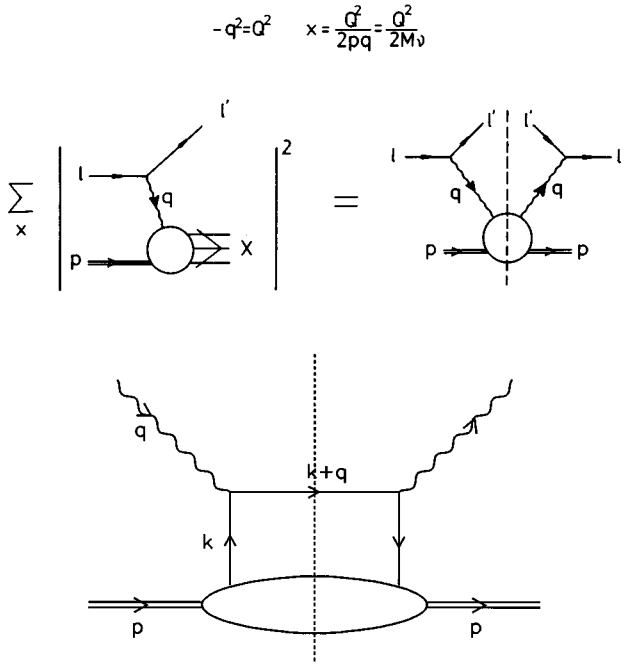


FIG. 2. (a) Kinematics of inelastic charged-lepton–proton scattering in the one-photon exchange approximation and its relation through the optical theorem to Compton scattering for the virtual photon; $p$ and $q$ denote the four-momenta of the proton and virtual photon, respectively. (b) Handbag diagram for virtual Compton scattering on a proton; $k$ denotes the four-momentum of the struck quark (antiquark). At high $Q^2$ and in the infinite-momentum frame of the proton, $k \approx xp$ where $x$ is the Bjorken scaling variable.

should be considered as an extension of the comprehensive small-$x$ physics review of Badełek, Charchuła, Krawczyk, and Kwieciński (1992), including a more detailed treatment of low-$Q^2$ problems. We shall be concerned exclusively with charged-lepton inelastic scattering. A recent review of problems specific to inelastic neutrino (and antineutrino) interactions has been presented by Kopeliovich and Maraga (1993). We shall also focus predominantly on the structure function $F_2$; particular final-state structures, such as jets, diffractive dissociation, and so on, will not be considered.

The content of the paper is as follows. After basic definitions and constraints (Sec. II) we present theoretical ideas and models describing low-$Q^2$ physics (Sec. III). High-energy photoproduction (Sec. IV) is then followed by a description of phenomenological parametrizations of structure functions (Sec. V). Special attention is given to dynamical models of the low-$Q^2$ behavior of $F_2$ (Sec. VI). Nuclear shadowing is described in Sec. VII, and finally, an update of experimental data is given in Sec. VIII. Section IX contains conclusions and outlook.

## II. BASIC DEFINITIONS AND CONSTRAINS

The kinematics of inelastic charged-lepton scattering is defined in Fig. 2(a). The one-photon exchange approximation is assumed throughout this paper. The imaginary part of the forward Compton scattering amplitude of the virtual photon is defined by the tensor $W^{\mu\nu}$ (see, for example, Halzen and Martin, 1984):

$$W^{\mu\nu}(p,q)=\frac{F_1(x,Q^2)}{M}\left(-g_{\mu\nu}+\frac{q^\mu q^\nu}{q^2}\right)+\frac{F_2(x,Q^2)}{M(p\cdot q)}\left(p^\mu-\frac{p\cdot q}{q^2}q^\mu\right)\left(p^\nu-\frac{p\cdot q}{q^2}q^\nu\right). \tag{1}$$

In this equation $q^2$ is the square of the four-momentum transfer, $Q^2=-q^2$, $x=Q^2/(2p\cdot q)$ is the Bjorken scaling variable, and $M$ is taken as the proton mass. The invariant quantity $p\cdot q$ is related to the energy transfer $\nu$ in the target rest frame by $p\cdot q=M\nu$. The invariant mass $W$ of the electroproduced hadronic system is then $W^2=M^2+2M\nu-Q^2$. Often one uses the notation $W^2\equiv s$.

The deep-inelastic regime is defined as a region where both $Q^2$ and $2M\nu$ are large, and their ratio $x$ is kept fixed. At $Q^2$ smaller than few $\mathrm{GeV}^2$, $x$ can probably no longer be interpreted as the momentum of a struck parton, but it remains a convenient variable for displaying the data. The functions $F_1(x,Q^2)$ and $F_2(x,Q^2)$ are the structure functions of the target. For a nuclear target it will be assumed that the structure functions are normalized to the number of nucleons in the target nucleus, and they will be denoted $F_i^A$, $i=1,2$ (except for the deuteron where the symbol $F_2^d$ will be used). The tensor $W^{\mu\nu}$ satisfies the current conservation constraints

$$q_\mu W^{\mu\nu}=0,$$
$$q_\nu W^{\mu\nu}=0. \tag{2}$$

This follows from the fact that $W^{\mu\nu}$ is related to a matrix element of the product of two electromagnetic current operators $j^\mu_{\rm em}(x)$:

$$W^{\mu\nu}\equiv \mathrm{Im}T^{\mu\nu}\propto \mathrm{Im}i\int d^4z\exp(iqz)\langle p|Tj^{\mu+}_{\rm em}(z)j^\nu_{\rm em}(0)|p\rangle, \tag{3}$$

where the symbol $T$ denotes time ordering.

Let us rearrange Eq. (1) in order to display explicitly the potential kinematic singularities of the tensor $W^{\mu\nu}$ at $Q^2=0$:

$$W^{\mu\nu}(p,q)=-\frac{F_1}{M}g^{\mu\nu}+\frac{F_2}{M(p\cdot q)}p^\mu p^\nu + \left(\frac{F_1}{M}+\frac{F_2}{M}\frac{p\cdot q}{q^2}\right)\frac{q^\mu q^\nu}{q^2}-\frac{F_2}{M}\frac{p^\mu q^\nu+p^\nu q^\mu}{q^2}. \tag{4}$$

These singularities cannot be real, and appear only as artifacts of the way we wrote $W^{\mu\nu}$. In order to eliminate them we impose the following conditions on the structure functions $F_i$ in the limit $Q^2\to 0$:

$$F_2=O(Q^2), \tag{5}$$

$$\frac{F_1}{M}+\frac{F_2}{M}\frac{p\cdot q}{q^2}=O(Q^2). \tag{6}$$

These conditions must be fulfilled for arbitrary $\nu$. They will play an important role in the parametrizations of the structure functions at low $Q^2$.

The differential electroproduction cross section is expressed in the following way using the structure functions $F_i$:

$$\frac{d^2\sigma(x,Q^2)}{dQ^2dx}=\frac{4\pi\alpha^2}{Q^4}\left[\left(1-y-\frac{Mxy}{2E}\right)\frac{F_2(x,Q^2)}{x} + \left(1-\frac{2m^2}{Q^2}\right)y^2F_1(x,Q^2)\right], \tag{7}$$

where $E$ denotes the energy of the incident lepton in the target rest frame, $m$ is the lepton mass, $y=\nu/E$, and $\alpha$ is the electromagnetic coupling constant.

Instead of $F_1$ the structure function $R(x,Q^2)$, defined as

$$R(x,Q^2)=\frac{\sigma_L}{\sigma_T}=\frac{(1+4M^2x^2/Q^2)F_2}{2xF_1}-1, \tag{8}$$

is often used; here $\sigma_L$ and $\sigma_T$ denote the cross sections for the longitudinally and transversally polarized virtual photons, respectively. The differential cross section (7) then reads

$$\frac{d^2\sigma(x,Q^2)}{dQ^2dx}=\frac{4\pi\alpha^2}{Q^4}\frac{F_2}{x}\left[1-y-\frac{Mxy}{2E} + \left(1-\frac{2m^2}{Q^2}\right)\frac{y^2(1+4M^2x^2/Q^2)}{2(1+R)}\right]. \tag{9}$$

Real photons are only transversally polarized, and therefore $\sigma_L$ and $R$ vanish when $Q^2\to 0$. This vanishing follows from Eqs. (5) and (6). The function $R$ is related to the frequently used longitudinal structure function $F_L(x,Q^2)$ via $R=F_L/2xF_1$, with

$$F_L(x,Q^2)=\left(1+\frac{4M^2x^2}{Q^2}\right)F_2-2xF_1. \tag{10}$$

At large $Q^2$, $F_L$ is directly sensitive to the gluon distribution function, which plays a crucial role in the interactions at small $x$ (Roberts, 1990).

## III. BASIC THEORETICAL CONCEPTS RELEVANT TO THE SMALL $Q^2$ REGION

In the leading $\log(Q^2)$ approximation of perturbative QCD, which is applicable in the high-$Q^2$ region, the structure function $F_2(x,Q^2)$ is directly related to the quark and antiquark momentum distributions $q_i(x,Q^2)$ and $\bar q_i(x,Q^2)$:

$$F_2(x,Q^2)=x\sum_i e_i^2[q_i(x,Q^2)+\bar q_i(x,Q^2)], \tag{11}$$

where $i$ labels the quark flavors and $e_i$ are the quark charges. The origin of this formula is illustrated in Fig. 2(b). For large $Q^2$ the Bjorken scaling variable $x$ acquires the meaning of the fraction of the proton momentum carried by a struck quark. In this region the quark and antiquark distributions exhibit approximate Bjorken scaling mildly violated by the QCD logarithmic corrections. The evolution of these distributions with $Q^2$ is described by the Altarelli-Parisi equations (Altarelli and Parisi, 1977; Reya, 1981; Altarelli, 1982). These equations as well as the relation (11) acquire corrections proportional to $\alpha_s(Q^2)$ in the next-to-leading $\log(Q^2)$ approximation.

Systematic analysis of the structure functions in the Bjorken limit can be carried out using the operator product expansion of the electromagnetic currents [see Eq. (3)] (Roberts, 1990). This expansion leads to expansion of the structure functions in inverse powers of $Q^2$:

$$F_2(x,Q^2)=\sum_{n=0}^{\infty}\frac{C_n(x,Q^2)}{(Q^2)^n}, \tag{12}$$

where the functions $C_n(x,Q^2)$ depend weakly (i.e., logarithmically) on $Q^2$. Terms in this expansion are referred to as leading ($n=0$) and higher ($n\geq 1$) twists. The twist number is defined such that the leading one is equal to two, and higher ones correspond to consecutive even integers.

Thus the right-hand side of Eq. (11), with approximate Bjorken scaling of quark distributions, corresponds to the leading twist contribution to the $F_2$. For moderately large values of $Q^2$ (on the order of a few $\mathrm{GeV}^2$) contributions of the higher twists may become significant. Contrary to common opinion, the higher twists are only corrections to the leading (approximately scaling) term (11) in the large-$Q^2$ region. Thus they cannot correctly describe the low-$Q^2$ (i.e., nonperturbative) region

since the expansion (12) gives a divergent series there. In particular, it should be noted that the individual terms in this expansion violate the constraint of Eq. (5). In order to describe this region correctly the (formal) expansion has to be summed beforehand, at large $Q^2$, and then continued to the region of $Q^2 \sim 0$. This is automatically accomplished in certain models such as the vector-meson dominance (VMD) model. To be precise, this model, together with its generalization which gives (approximate) scaling at large $Q^2$, can be represented in the form of Eq. (12) for sufficiently large $Q^2$.

The VMD model is a quantitative realization of the experimental fact that photon interactions are often similar to those of a hadron (Bauer, Spital, Yennie, and Pipkin, 1978; Grammer and Sullivan, 1978). The structure function $F_2$ is represented in this model by

$$F_2[x=Q^2/(s+Q^2-M^2),Q^2]=\frac{Q^2}{4\pi}\sum_v \frac{M_v^4\sigma_v(s)}{\gamma_v^2(Q^2+M_v^2)^2}, \tag{13}$$

where the quantities $\sigma_v(s)$ are the vector-meson–nucleon total cross sections, $M_v$ is the mass of the vector meson $v$, and $\gamma_v^2$ can be related in the standard way to the leptonic width of the $v$ (Bauer, Spital, Yennie, and Pipkin, 1978):

$$\frac{\gamma_v^2}{\pi}=\frac{\alpha^2 M_v}{3\Gamma_{e^+e^-}}. \tag{14}$$

If only a finite number of vector mesons is included in the sum (13), then $F_2$ vanishes as $1/Q^2$ at large $Q^2$. Therefore it does not contain the leading twist term. Scaling can be introduced by including an infinite number of vector mesons in the sum. This version of the VMD model is called the generalized VMD model (Bauer, Spital, Yennie, and Pipkin, 1978; Grammer and Sullivan, 1978). The heavy-meson contribution is directly related to the structure function in the scaling region.

In practical applications to the analysis of experimental data which extend to moderate values of $Q^2$, one often includes the higher-twist corrections in the following simplified way:

$$F_2(x,Q^2)=F_2^{\mathrm{LT}}(x,Q^2)\left[1+\frac{H(x)}{Q^2}\right], \tag{15}$$

where the $F_2^{\mathrm{LT}}$ is the leading-twist contribution to $F_2$, and $H(x)$ is determined from a fit to the data. This simple-minded expression may not be justified theoretically, since in principle the higher-twist terms, i.e., the functions $C_n(x,Q^2)$ for $n \geqslant 1$ in Eq. (12), evolve differently with $Q^2$ than the leading-twist term.

At high energies, Regge theory (Collins, 1977) is often used to parametrize the cross sections as functions of energy $W$. The high-energy behavior of the total cross sections is then given by the following expression:

$$\sigma_t(W)=\sum_i \beta_i (W^2)^{\alpha_i-1}, \tag{16}$$

where $\alpha_i$ are the intercepts of the Regge poles, and $\beta_i$ denote their couplings. The intercepts $\alpha_i$ are universal quantities, i.e., they are independent of the external particles or currents and depend only on the quantum numbers of the Regge poles exchanged in the crossed channel. Regge-pole exchange is to a large extent a generalization of particle exchange, and formally describes a pole of the partial-wave amplitude in the crossed channel in the complex angular momentum plane. The Regge pole corresponding to the vacuum quantum numbers is called Pomeron. It is expected to have the highest intercept, close to unity. It is a phenomenologically established fact that the energy dependence of the total hadronic and photoproduction cross sections can be described by two contributions, the (effective) Pomeron with intercept $\alpha_P \cong 1.08$ and the Reggeon with the intercept $\alpha_R$ close to 0.5 (Donnachie and Landshoff, 1992). Since the bulk of the cross sections comes from soft processes, one usually refers to the phenomenological Pomeron having its intercept slightly above unity as the soft Pomeron. On the other hand, in the leading logarithmic approximation of perturbative QCD one finds the Pomeron to have intercept significantly above unity (Kuraev, Lipatov, and Fadin, 1977; Balitskij and Lipatov, 1978; Bronzan and Sugar, 1978; Jaroszewicz, 1980; Gribov, Levin, and Ryskin, 1983; Ciafaloni, 1988; Lipatov, 1989; Catani, Fiorani, and Marchesini, 1990a, 1990b). Since perturbative QCD is only applicable to the description of hard processes, one refers to this QCD Pomeron as the hard Pomeron. Its relation to and interplay with the phenomenologically determined soft Pomeron is still not fully understood. It should also be emphasized that the Pomeron with intercept above unity leads to violation of unitarity at asymptotic energies. The unitarity is restored by multiple-scattering absorptive (or shadowing) terms.

The Regge parametrization of the total cross sections implies the following parametrization of the electroproduction structure function $F_2(x,Q^2)$:

$$F_2(x,Q^2)=\sum_i \beta_i(Q^2)(W^2)^{\alpha_i-1}. \tag{17}$$

This is expected to be valid in the high-energy limit and for $W^2 \gg Q^2$. In this limit $x \simeq Q^2/W^2$ and $x \ll 1$. Therefore the Regge parametrization (17) implies the following small-$x$ behavior of $F_2(x,Q^2)$:

$$F_2(x,Q^2)=\sum_i \tilde{\beta}_i(Q^2)x^{1-\alpha_i}, \tag{18}$$

where

$$\tilde{\beta}_i(Q^2)=(Q^2)^{\alpha_i-1}\beta_i(Q^2). \tag{19}$$

At low $Q^2$ the functions $\beta_i(Q^2)$ should obey the constraint of Eq. (5), i.e., $\beta_i(Q^2)=O(Q^2)$ for $Q^2 \to 0$.

## IV. HIGH-ENERGY PHOTOPRODUCTION

The low-$Q^2$ region should join smoothly onto the photoproduction limit, $Q^2=0$. In this limit one has the

following relation between the total photoproduction cross section $\sigma_{\gamma p}(E_\gamma)$ and the structure function $F_2$:

$$\sigma_{\gamma p}(E_\gamma)=\lim_{Q^2\to 0} 4\pi^2\alpha\frac{F_2}{Q^2}. \tag{20}$$

The limit should be taken at fixed $\nu=E_\gamma$, where $E_\gamma$ is the photon energy in the laboratory frame. Several structure function parametrizations use the total photoproduction cross section as an additional constraint.

When considering photoproduction it is conventional to decompose the total cross section $\sigma_{\gamma p}$ into two parts,

$$\sigma_{\gamma p}=\sigma_{\rm VMD}+\sigma_{\rm part}, \tag{21}$$

and

$$\sigma_{\rm part}=\sigma_{\rm direct}+\sigma_{\rm anomalous}. \tag{22}$$

In this equation, $\sigma_{\rm VMD}$ denotes the cross section corresponding to the VMD photon-hadron interaction mechanism, and $\sigma_{\rm part}$ denotes that corresponding to the partonic mechanism. In order to avoid double counting, $\sigma_{\rm VMD}$ contains contributions from light vector mesons only (see Sec. III). The partonic component of the cross section is next decomposed into two terms, the "direct" term, which reflects photon interactions with the partonic constituents of the hadron, and the "anomalous" term, which corresponds to the interactions of the partonic constituents of the photon with the partonic constituents of the hadron. In the latter case the photon's coupling to its constituents is pointlike. The main feature of the partonic mechanism is that it corresponds to (semi) hard interactions which can be described by perturbative QCD. The VMD part, on the other hand, contains both hard and soft components. The former come from the hard interaction between the parton constituents of the vector meson. Unlike the anomalous part this term cannot be described by perturbative QCD alone, since its description requires knowledge of the (nonperturbative) parton distributions in the vector meson. The anomalous term, together with the hard part of the VMD contribution, represents the pointlike interaction of the partonic constituents of the photon. In the literature the corresponding events are therefore called the "resolved" photon events (Abramowicz, Charchuła, Krawczyk, Levy, and Maor, 1993; Levy, 1993; Schuler and Sjöstrand, 1993; Storrow, 1993).

It follows from Eq. (20) that the total photoproduction cross section can be obtained from extrapolation of $F_2/Q^2$ to $Q^2=0$. The partonic component $\sigma_{\rm part}$ (i.e., the sum of the direct and anomalous terms) can be identified with the difference between the result of the extrapolation and the VMD part (Schuler and Sjöstrand, 1993). The most important distinction between the various mechanisms appears through analysis of the final states, which will not be discussed here (see Schuler and Sjöstrand, 1993).

The total photoproduction cross section, like the hadron-hadron total cross sections, exhibits an increase with increasing photon energy [Alekhin *et al.*, 1987; Derrick *et al.* (ZEUS Collaboration), 1992, 1994; Ahmed *et al.* (H1 Collaboration), 1993]; see Fig. 3. This increase

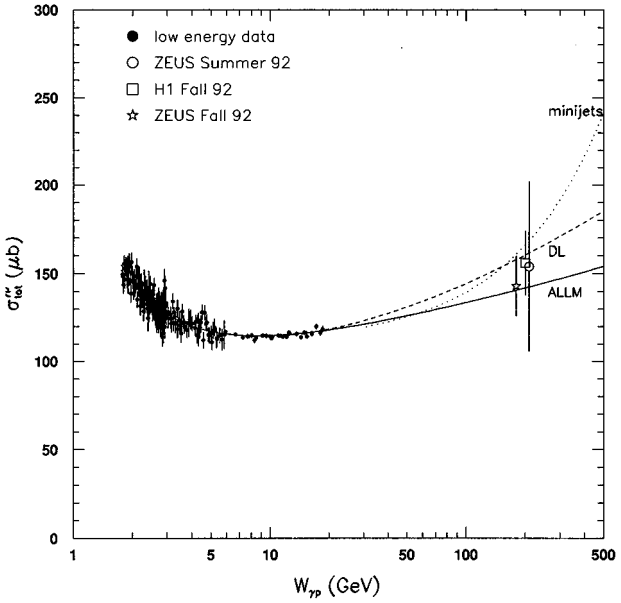


FIG. 3. Total photoproduction cross section as a function of the $\gamma p$ center-of-mass energy $W_{\gamma p}$. Low-energy data come from Alekhin *et al.* (1987), recent ZEUS Collaboration data from Derrick *et al.* (1994), and previous data from Derrick *et al.* (ZEUS Collaboration) (1992) and Ahmed *et al.* (H1 Collaboration) (1993). The curves are explained in the text. From Derrick *et al.* (ZEUS Collaboration) (1994).

is well described by a soft Pomeron contribution with intercept equal to 1.08 (Donnachie and Landshoff, 1992) (see also Sec. III). It is also well described by an extrapolation of the parametrization of Abramowicz *et al.* (Abramowicz, Levin, Levy, and Maor, 1991). Both predictions are shown in Fig. 3. Another possible description of the total cross-section increase is provided by minijet production, i.e., production of jets with relatively low $p_T$ (beginning from 1–2 GeV or so). Minijet production is described by the hard scattering of partons coming from the photon and proton. The energy dependence of the cross section reflects to a large extent the small-$x$ behavior of the parton (i.e., mostly gluon) distributions in a proton and in a photon. This follows from the kinematics of hard parton-parton scattering:

$$x_1x_2W^2_{\gamma p}\geq 4p_T^2, \tag{23}$$

where $x_{1,2}$ denote the momentum fractions carried by partons, and $W_{\gamma p}$ is the total c.m. energy. For increasing $W_{\gamma p}$ (and for fixed $p_T^2$), $x_1$ and $x_2$ may assume smaller values. The magnitude of the cross section is sensitive to the magnitude of the minimal value of $p_T$. It can be shown that the multiple-scattering (or absorptive) corrections are extremely important here and that they significantly slow the increase of the total cross section with energy (Ghandi, Sarcevic, Burrows, Durand, and Pi, 1990; Forshaw and Storrow, 1991 (and erratum), 1994; Forshaw, 1992; Honjo, Durand, Ghandi, Pi, and Sarcevic, 1993; Schuler and Sjöstrand, 1993; Storrow, 1993). A possible prediction for the total cross-section energy dependence following from the minijet produc-

tion picture is shown in Fig. 3 [see Derrick *et al.* (ZEUS Collaboration), 1994 for the details].

A global quantity like the total cross section cannot discriminate between different models, and the detailed structure of the final states may be crucial here. The relevant Monte Carlo event generator for the minijet model with multiple scattering is discussed by Butterworth and Forshaw (1993).

## V. PHENOMENOLOGICAL PARAMETRIZATIONS OF STRUCTURE FUNCTIONS

There exist several phenomenological parametrizations of the structure functions which incorporate the $Q^2\to 0$ constraints (see Sec. II) as well as the Bjorken scaling behavior at large $Q^2$ [Brasse, Flanger, Gyler, Goel, Haidan, Merkowitz, and Wriedt, 1976; Gordon *et al.* (CHIO Collaboration), 1979; Donnachie and Landshoff, 1984, 1994; Amaudruz *et al.* (NMC), 1992d; Abramowicz, Levin, Levy, and Maor, 1993; Capella *et al.*, 1994; Merino, 1994]. Certain parametrizations [Abramowicz, Levin, Levy, and Maor, 1991; Amaudruz *et al.* (NMC), 1992d; Capella, Kaidalov, Merino, and Trân Thanh Vân, 1994; Merino, 1994] also contain the (QCD-motivated) scaling violations. The parametric form of the corresponding $Q^2$ dependence, however, is usually [Abramowicz, Levin, Levy, and Maor, 1991; Amaudruz *et al.* (NMC), 1992d] not constrained at large $Q^2$ by the Altarelli-Parisi evolution equations, i.e., those parametrizations are not linked with the conventional QCD evolution. Nor is the low-$Q^2$ behavior related to the explicit vector-meson dominance, known to occur at low $Q^2$ (Bauer, Spital, Yennie, and Pipkin, 1978).

The parametrization used by the CHIO Collaboration (Gordon *et al.*, 1979) to fit their high-energy muon-proton and muon-deuteron data includes the low-$x$ and low-$Q^2$ region. It is a combination of a simple parton model (valence quarks) and the generalized VMD approach (sea quarks):

$$F_2(x,Q^2)=P_3(2+g_3)x(1-x)^{1+g_3} + P_5\frac{14}{9}\frac{4+g_5}{5+g_5}(1-x)^{1+g_5}\frac{Q^2}{Q^2+m_0^2}, \tag{24}$$

where $g_3=g_{03}+\varepsilon$, $g_5=g_{05}+\varepsilon$, $\varepsilon=\kappa\ln[(Q^2+m_0^2)/m_0^2]$, and $P_3, P_5, g_{03}, g_{05}, \kappa$, and $m_0$ are free parameters. This parametrization is obsolete and is mentioned here for historical reasons only. On the other hand, the CHIO data are still being used in fits describing the low $x$-region (see the NMC parametrization below).

The parametrization of Brasse *et al.* (Brasse, Flanger, Gyler, Goel, Haidan, Merkowitz, and Wriedt, 1976) describes a wealth of data on virtual photon-proton scattering in the resonance region of $0.1\leqslant Q^2\leqslant 6$ GeV$^2$, $1.11\leqslant W\leqslant 1.99$ GeV (see Fig. 1). It is used in radiative-corrections calculations by, among others, the E665 experiment at Fermilab. The virtual Compton scattering cross section is assumed to be

$$\sigma(Q^2,W,\epsilon)=\sigma_T(Q^2,W)+\epsilon\sigma_L(Q^2,W), \tag{25}$$

where the parameter $\epsilon$ denotes the degree of polarization of the virtual photon, and the cross sections $\sigma_T(Q^2,W)$ and $\sigma_L(Q^2,W)$ are related in a standard way to the structure functions $F_2$ and $F_L$, namely,

$$F_2=\frac{Q^2}{4\pi^2\alpha}(\sigma_T+\sigma_L), \tag{26}$$

$$F_L=\frac{Q^2}{4\pi^2\alpha}\sigma_L. \tag{27}$$

The cross section $\sigma(Q^2,W,\epsilon)$ is parametrized in the following way:

$$\ln(\sigma/G^2)=a(W)+b(W)\ln\frac{|\mathbf{q}|}{|\mathbf{q}_0|}+c(W)\left|\ln\frac{|\mathbf{q}|}{|\mathbf{q}_0|}\right|^{d(W)}, \tag{28}$$

where $\mathbf{q}$ is the three-momentum transfer to the hadronic system, i.e., $|\mathbf{q}|=\sqrt{Q^2+\nu^2}$, $|\mathbf{q}_0|$ is the value of $|\mathbf{q}|$ for $Q^2=0$, i.e., $|\mathbf{q}_0|=(W^2-M^2)/2M$, and $G^2(Q^2)$ is the dipole form factor of the nucleon, i.e.,

$$G^2(Q^2)=\left(\frac{1}{1+Q^2/0.71\text{GeV}^2}\right)^2. \tag{29}$$

The parameters of $a(W)$, $b(W)$, $c(W)$, and $d(W)$ were obtained from a fit to the data in different bins of $W$. Their values are tabulated (Brasse, Flanger, Gyler, Goel, Haidan, Merkowitz, and Wriedt, 1976).

A complete parametrization of $F_2^d$ including the resonance region was obtained by the New Muon Collaboration (NMC) (Amaudruz *et al.*, 1992d) to perform the radiative-corrections calculations. It is being used by other deep-inelastic scattering experiments too, like the SMC at CERN and the E665 experiment at Fermilab. Thus we shall list the values of all its parameters here. In the resonance region $F_2^d$ was fitted to the data from SLAC (Mestayer, 1978) taking into account only the $\Delta(1232)$ resonance. Outside the resonance region a QCD-based parametrization was used to describe the data of CHIO (Gordon *et al.*, 1979), SLAC (Whitlow, Riordan, Dasu, Rock, and Bodek, 1992), BCDMS (Benvenuti *et al.*, 1989, 1990) and EMC NA28 (Arneodo *et al.*, 1990). For this purpose, the structure function was parametrized as

$$F_2^d(x,Q^2)-[1-G^2(Q^2)][F^{\text{dis}}(x,Q^2)+F^{\text{res}}(x,Q^2) + F^{\text{bg}}(x,Q^2)], \tag{30}$$

where $F^{\text{dis}}$ and $F^{\text{res}}$ are the contributions from the deep-inelastic and resonance regions, respectively, and $F^{\text{bg}}$ describes the background under the resonance. The nucleon electromagnetic form factor is given by Eq. (29); the factor $1-G^2$ in Eq. (30) suppresses $F_2$ at low values of $Q^2$, where elastic scattering on the nucleon dominates.

The contribution from the deep-inelastic region was parametrized as

$$F^{\rm dis}(x,Q^2)=\left[\frac{5}{18}\frac{3}{B(\eta_1,\eta_2+1)}x_w^{\eta_1}(1-x_w)^{\eta_2}+\frac{1}{3}\eta_3(1-x_w)^{\eta_4}\right]S(x,Q^2), \quad (31)$$

where $x_w=(Q^2+m_a^2)/(2m\nu+m_b^2)$ with $m_a^2=0.351$ GeV$^2$ and $m_b^2=1.512$ GeV$^2$. The quantity $B$ is the Euler beta function and $\eta_1,\ldots,\eta_4$ are linear functions of the variable $\bar{s}$,

$$\eta_i=\alpha_i+\beta_i\bar{s}, \quad (32)$$

where

$$\bar{s}=\ln\frac{\ln[(Q^2+m_a^2)/\Lambda^2]}{\ln[(Q_0^2+m_a^2)/\Lambda^2]}, \quad (33)$$

with $Q_0^2=2.0$ GeV$^2$ and $\Lambda=0.2$ GeV. The constants $\alpha_1,\ldots,\alpha_4$ and $\beta_1,\ldots,\beta_4$ were free parameters in the fit.

The factor $S(x,Q^2)$ in Eq. (31) suppresses $F^{\rm dis}$ in the resonance region close to the single-pion production threshold:

$$S(x,Q^2)=1-e^{-a(W-W_{\rm thr})}, \quad (34)$$

with $W_{\rm thr}=1.03$ GeV and $a=4.177$ GeV$^{-1}$.

The form adopted for the contribution from the resonance region was

$$F^{\rm res}(x,Q^2)=\alpha_5^2G^{3/2}e^{-(W-m_\Delta)^2/\Gamma^2}, \quad (35)$$

with $m_\Delta=1.232$ GeV, $\Gamma=0.0728$ GeV, and $\alpha_5$, a free parameter in the fit, set equal to 0.894 56. This parametrization takes into account only the $\Delta(1232)$ contribution; higher-mass resonances are neglected.

The background under the resonance region was parametrized as

$$F^{\rm bg}(x,Q^2)=\alpha_6^2G^{1/2}\xi e^{-b(Q-W_{\rm thr})^2}, \quad (36)$$

where

$$\xi=\sqrt{\frac{[(W+c)^2+M^2-m_\pi^2]^2}{4(W+c)^2}-M^2}, \quad (37)$$

with $b=0.5$ GeV$^{-1}$ and $c=0.05$ GeV. The parameter $\alpha_6$, left free in the fit, was equal to 0.164 52.

The parametrization (30) of the function $F_2^d$ is valid from $Q^2\sim0$ up to about 200 GeV$^2$, and from $x=0.003$ up to 0.7. However, the results of the fit given in Amaudruz *et al.* (NMC) (1992d) are obsolete since the new $F_2$ measurements by the NMC (Amaudruz *et al.*, 1992b, 1992c, 1995; Arneodo *et al.*, 1995a), which were not included in the fit, differ by up to 30% from the former world data. When used later in the radiative-corrections procedure, the deep-inelastic part of $F_2$ was refitted, while the parametrization of the resonances and the background was kept fixed. Two types of the former were used, 8- and 15-parameter functions. The 15-parameter function and the fitted values of its coefficients are given in Table I (Arneodo *et al.*, 1995a).

A low-$Q^2$ parametrization of $F_2^p$ was obtained by Donnachie and Landshoff (Donnachie and Landshoff, 1985). In this parametrization, the parton model is extrapolated down to the region of low $Q^2$ (including the photoproduction), respecting the constraints discussed in Sec. II. The parametrizations of the sea- and valence-quark distributions at small values of $x$ are based on Regge theory (see Sec. III) and correspond to a Pomeron intercept of approximately 1.08 and Reggeon intercept about 0.5. The structure function $F_2^p$ is given by the conventional parton-model formula

$$F_2^p=x\left(\frac{4}{9}(u+\bar{u})+\frac{1}{9}(d+\bar{d})+\frac{1}{9}\lambda(s+\bar{s})\right), \quad (38)$$

where $u,\bar{u},\ldots,$ are the parton densities, and $\lambda$ measures the reduced strength of the Pomeron's coupling to strange quarks ($\lambda\approx0.6$). The individual parton densities are related in the following way to the sea- and valence-quark distributions $S(x)$ and $V(x)$:

$$\begin{aligned}
&xu(x)=S(x)+2V(x),\quad xd(x)=S(x)+V(x),\\
&xs(s)=S(x),\\
&x\bar{u}(x)=x\bar{d}(x)=x\bar{s}(x)=S(x),\\
&F_2(x,Q^2)=A(x)\cdot\left[\frac{\ln(Q^2/\Lambda^2)}{\ln(Q_0^2/\Lambda^2)}\right]^{B(x)}\cdot\left[1+\frac{C(x)}{Q^2}\right],\\
&Q_0^2=20\ \text{GeV}^2,\quad \Lambda=250\ \text{MeV},\\
&A(x)=x^{a_1}(1-x)^{a_2}[a_3+a_4(1-x)+a_5(1-x)^2\\
&\qquad +a_6(1-x)^3+a_7(1-x)^4],\\
&B(x)=b_1+b_2x+b_3/(x+b_4),\\
&C(x)=c_1x+c_2x^2+c_3x^3+c_4x^4.
\end{aligned} \quad (39)$$

The densities $S(x)$ and $V(x)$ are parametrized as follows:

TABLE I. The parametrization of $F_2^p$ and $F_2^d$ [Arneodo *et al.* (NMC), 1995a]. This function is strictly valid only in the kinematic range of the NMC, SLAC, and BCDMS data, $0.006<x<0.9$ and $0.5<Q^2<200$ GeV$^2$.

| Parameter | proton | deuteron |
|---|---|---|
| $a_1$ | −0.02778 | −0.04858 |
| $a_2$ | 2.926 | 2.863 |
| $a_3$ | 1.0362 | 0.8367 |
| $a_4$ | −1.840 | −2.532 |
| $a_5$ | 8.123 | 9.145 |
| $a_6$ | −13.074 | −12.504 |
| $a_7$ | 6.215 | 5.473 |
| $b_1$ | 0.285 | −0.008 |
| $b_2$ | −2.694 | −2.227 |
| $b_3$ | 0.0188 | 0.0551 |
| $b_4$ | 0.0274 | 0.0570 |
| $c_1$ | −1.413 | −1.509 |
| $c_2$ | 9.366 | 8.553 |
| $c_3$ | −37.79 | −31.20 |
| $c_4$ | 47.10 | 39.98 |

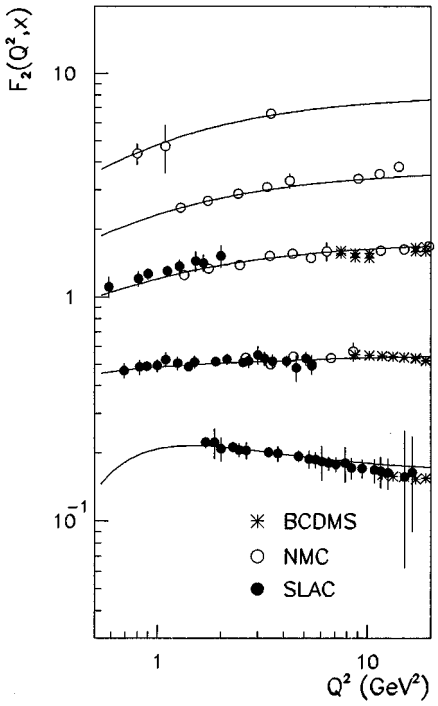


FIG. 4. Parametrization of $F_2^p(x,Q^2)$ by Donnachie and Landshoff as a function of $Q^2$ for the following values of $x$ (from the top): 0.008, 0.035, 0.07, 0.18, and 0.45, together with data from the NMC (Amaudruz *et al.*, 1992b, 1992c), SLAC (Whitlow, Riordan, Dasu, Rock, and Bodek, 1992), and BCDMS (Benvenuti *et al.*, 1989, 1990). The $F_2$ values are scaled for clarity by the factors (from the top) 16, 8, 4, 1.5, and 1. The error bars represent statistical and systematic errors added in quadrature. From Badełek, Bentvelsen, Kooijman, Kwieciński, Spiesberger, and von Schlippe, 1993.

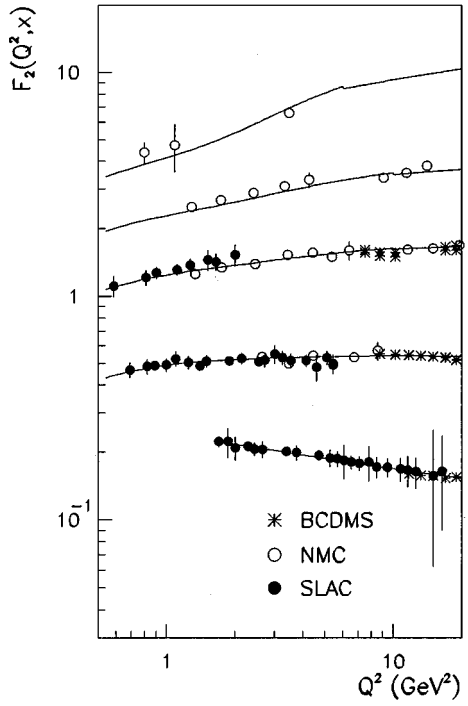


FIG. 5. Parametrization of $F_2^p(x,Q^2)$ by Abramowicz *et al.*. The $x$ values, data, and scaling factors are as in Fig. 4. From Badełek, Bentvelsen, Kooijman, Kwieciński, Spiesberger, and von Schlippe, 1993.

$$S(x)=0.17x^{-0.08}(1-x)^5,$$
$$V(x)=1.33x^{0.56}(1-x)^3. \tag{40}$$

The functions $S(x)$ and $V(x)$ are next multiplied by the factors $\phi_s(Q^2)$ and $\phi_v(Q^2)$, respectively, where

$$\phi_s(Q^2)=\left(\frac{Q^2}{Q^2+0.36}\right)^{1.08},$$
$$\phi_v(Q^2)=\left(\frac{Q^2}{Q^2+0.85}\right)^{0.44}. \tag{41}$$

The powers are chosen so as to make $F_2^p$ vanish like $Q^2$ as $Q^2\to 0$.

The Donnachie and Landshoff parametrization has recently been extended and modified (Donnachie and Landshoff, 1994) to include in more detail the heavy-quark contribution and the region of large $x$. Instead of the scaling variable $x$ one uses

$$\xi_i=x\left(1+\frac{\mu_i^2}{Q^2}\right), \tag{42}$$

where the index $i$ labels charmed, strange, and light quarks. Strangeness and charm distributions are as follows:

$$xs(x,Q^2)=C_s\frac{Q^2}{Q^2+a_s}\xi_s^{-\epsilon}(1-\xi_s)^7,$$
$$xc(x,Q^2)=C_c\frac{Q^2}{Q^2+a_c}\xi_c^{-\epsilon}(1-\xi_c)^7, \tag{43}$$

where $C_s\approx 0.22$, $C_c=0.032$, $a_s=1$ GeV$^2$, $a_c=6.25$ GeV$^2$, and $\epsilon=0.0808$. The parameters $\mu_{s,c}^2$ defining the variables $\xi_{s,c}$ [see Eq. (42)] are $\mu_s^2=1.7$ GeV$^2$ and $\mu_c^2=16$ GeV$^2$.

Parametrization of the light-quark distributions is more involved, i.e., different functional forms obtained from a fit to the data are used for $\xi$ smaller and greater than a certain $\xi_0$, which is a free parameter in the fit. The valence-quark distributions are parametrized as follows:

$$xu_v(x,Q^2)=U(\xi)\psi(Q^2),$$
$$U(\xi)=B_u\xi^{0.4525}, \quad \xi<\xi_0 \tag{44}$$

and

$$xd_v(x,Q^2)=D(\xi)\psi(Q^2),$$
$$D(\xi)=B_d\xi^{0.4525}, \quad \xi<\xi_0,$$
$$D(\xi)=\beta_d\xi^{\lambda_d}(1-\xi)^4, \quad \xi>\xi_0. \tag{45}$$

The parameter $\mu^2$ defining the variable $\xi$ for light quarks is $\mu^2=0.28$ GeV$^2$. Parameters $B_{u,d}$, $\beta_{u,d}$, and $\lambda_{u,d}$ are fixed by requiring that the two functional forms defining $U(\xi)$ and $D(\xi)$ join smoothly at $\xi_0$, and by

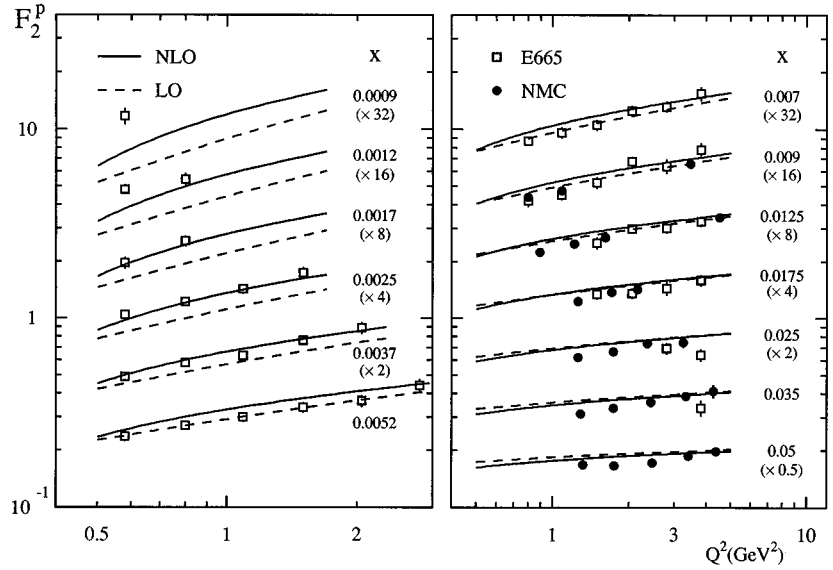


FIG. 6. Glück, Reya, and Vogt leading-twist calculations in leading- (dashed curve) and next-to-leading (solid curve) order for the $F_2^p$ compared to NMC data (Amaudruz *et al.*, 1992b, 1992c) and E665 data (Kotwal *et al.*, 1995; Kotwal, 1995). From Glück, Reya, and Vogt (1995) and Vogt (1995).

imposing the number sum rules. The function $\psi$ is $\psi(Q^2)=Q^2/(Q^2+b)$. The light sea-quark distributions are

$$q_S(x,Q^2)=C\xi^{-0.0808}\Phi(Q^2), \quad \xi<\xi_0,$$
$$q_S(x,Q^2)=\gamma\xi^{\lambda_S}(1-\xi)^7\Phi(Q^2), \quad \xi>\xi_0, \tag{46}$$

where $\Phi(Q^2)=Q^2/(Q^2+a)$. The parameters $C$, $a$, and $b$ are fixed by fitting to the data on photo- and electroproduction. The model also contains a Regge-like term in the sea-quark distributions which behaves like $\xi^{0.4525}$ at small $x$. It also contains an extra higher-twist term in the $F_2$ which is parametrized as follows:

$$ht(x,Q^2)=D\frac{x^2(1-\xi)^2}{1+Q^2/Q_0^2}. \tag{47}$$

The values of other parameters defining the model are given in Donnachie and Landshoff (1994). The parametrization is valid for $0\leqslant Q^2<10$ GeV$^2$ and for $x\geqslant 0.008$. It is being used in radiative-corrections calculations in deep-inelastic scattering experiments, for example, by the E665 experiment at Fermilab and by the NMC at CERN.

The function $F_2^p(x,Q^2)$ resulting from the parametrization of Donnachie and Landshoff is shown in Fig. 4, together with the data.

The parametrization proposed by Abramowicz *et al.* (Abramowicz, Levin, Levy, and Maor, 1991) is a result of a fit to structure-function data sets from SLAC (Whitlow, Riordan, Dasu, Rock, and Bodek, 1992), BCDMS (Benvenuti *et al.*, 1989, 1990), and EMC NA28 (Arneodo *et al.*, 1990), and to the then-available photoproduction cross section. The fitted function is based on the parton model with the QCD-motivated scaling violation appropriately extrapolated to the region of low $Q^2$ (including the photoproduction). Regge ideas are used in the parametrization.

The structure function $F_2$ is decomposed into two terms, $F_2^P$ and $F_2^R$, corresponding to Pomeron and Reggeon exchange,

$$F_2=F_2^P+F_2^R, \tag{48}$$

with each of them expressed as follows:

$$F_2^r=\frac{Q^2}{Q^2+m_0^2}C_r(t)x_r^{a_r(t)}(1-x)^{b_r(t)}, \tag{49}$$

where

$$\frac{1}{x_r}=\frac{2M\nu+m_r^2}{Q^2+m_r^2} \tag{50}$$

and $r=P,R$ stands either for Pomeron or for Reggeon. The argument of the functions $C_r(t)$, $a_r(t)$, and $b_r(t)$ is defined as

$$t=\ln\left(\frac{\ln[(Q^2+Q_0^2)/\Lambda^2]}{\ln(Q_0^2/\Lambda^2)}\right). \tag{51}$$

The functions $C_R$, $b_R$, $a_R$, and $b_P$, which increase with $Q^2$, were assumed to be of the form

$$p(t)=p_1+(p_1-p_2)t^{p_3}, \tag{52}$$

while the functions $C_P$ and $a_P$ were assumed to have the form

$$p(t)=p_1+(p_1-p_2)\left(\frac{1}{1+t^{p_3}}-1\right). \tag{53}$$

The parameters $m_0^2$, $m_r^2$, and $Q_0^2$, as well as the parameters $a_i$, $b_i$, and $C_i$ (separately for the Pomeron and the Reggeon terms, $i=1,2,3$), were obtained from the fit to the data.

The fit of Abramowicz *et al.* is valid from $Q^2=0$ up to the highest $Q^2$ values obtained in the fixed-target experiments, excluding the resonance region $W<1.75$ GeV. The structure function $F_2^p(x,Q^2)$ following from this representation is shown in Fig. 5. The fit given in Abramowicz, Levin, Levy, and Maor (1993) has recently been updated to incorporate the latest data on $F_2$ obtained by the NMC (Arneodo *et al.*, 1995a) and by the E665 collaboration (Kotwal *et al.*, 1995; Kotwal, 1995; Abramowicz, 1995).

The parametrization of Capella *et al.* (Capella, Kaidalov, Merino, and Trân Thanh Vân, 1994; Merino, 1994) is based on a fit to fixed-target data and large-$Q^2$ data from HERA [Abt *et al.* (H1 Collaboration), 1993; Derrick *et al.* (ZEUS Collaboration), 1993; Müller (H1 Collaboration), 1994; Roco (ZEUS Collaboration), 1994], which show a significant increase of $F_2$ with decreasing $x$. It also uses data on the photoproduction cross section, including the highest-energy results from HERA [Derrick *et al.* (ZEUS Collaboration), 1992, 1994; Ahmed *et al.* (H1 Collaboration), 1993]. This parametrization assumes a Regge form for $F_2$ at small $x$ and counting rules at large $x$. The leading small-$x$ behavior corresponding to the Pomeron is parametrized by the $Q^2$-dependent effective Pomeron intercept $1+\Delta(Q^2)$, which interpolates between the soft Pomeron at $Q^2=0$ and the hard one at large $Q^2$. The unusual $Q^2$ dependence of the effective Pomeron intercept is meant to describe in a phenomenological way the absorptive corrections to $F_2$, which are expected to be strong at low $Q^2$ values. The small-$x$ behavior corresponding to the Reggeon contribution is parametrized in a conventional way [see Eqs. (18) and (19)]. To be precise, the structure function $F_2(x,Q^2)$ is parametrized in the following form:

$$F_2(x,Q^2)=Ax^{-\Delta(Q^2)}(1-x)^{n(Q^2)+4}\left(\frac{Q^2}{Q^2+a}\right)^{1+\Delta(Q^2)} + Bx^{1-\alpha_R}(1-x)^{n(Q^2)}\left(\frac{Q^2}{Q^2+b}\right)^{\alpha_R}. \tag{54}$$

The first term corresponds to the Pomeron contribution with the effective Pomeron intercept parametrized as

$$\Delta(Q^2)=\Delta_0\left(1+\frac{2Q^2}{Q^2+d}\right) \tag{55}$$

with $\Delta_0\sim 0.08$, corresponding to the intercept of the soft Pomeron. The second term in (54) corresponds to the Reggeon contribution and at large $Q^2$ may be identified with the valence quarks. The Pomeron part corresponds to the sea-quark contribution at large $Q^2$. The function $n(Q^2)$ is parametrized as follows:

$$n(Q^2)=\frac{3}{2}\left(1+\frac{Q^2}{Q^2+c}\right). \tag{56}$$

Parameters $A$, $B$, $a$, $b$, $c$, and $d$ are obtained from the fit to the data. The parametrization (54) is used for moderately small and small $Q^2$ (including photoproduction, i.e., $Q^2=0$). The region of large $Q^2$ is described by a combination of this parametrization with the Altarelli-Parisi evolution equations.

## VI. DYNAMICAL MODELS OF THE LOW-$Q^2$ BEHAVIOR OF $F_2$

In the preceding section we have presented various parametrizations of the structure functions. These parametrizations, although motivated dynamically, were not linked with conventional QCD evolution at large $Q^2$ (the parametrization of Capella *et al.* is an exception; see Capella, Kaidalov, Merino, and Trân Than Vân, 1994; Merino, 1994); nor was the low-$Q^2$ dynamics explicitly taken into account. In this section we present parametrizations that will contain the QCD evolution. One of them will also include the VMD dynamics, which dominates at low $Q^2$.

The dynamically calculated structure functions of Glück, Reya, and Vogt (Glück, Reya, and Vogt, 1992, 1993, 1995; Glück and Reya, 1993) extend the QCD evolution equations down to the very-low-$Q^2$ region ($Q^2<1$ GeV$^2$). The parton distributions are calculated by evolving from the input valencelike distributions provided at the very low scale $\mu^2=0.3$ GeV$^2$, and both the leading and next-to-leading order approximations are used. The valencelike shape at the scale $\mu^2$ is assumed not only for the valence quarks, but also for gluon and sea-quark distributions:

$$xg(x,\mu^2)=Ax^{\alpha}(1-x)^{\beta},\quad x\bar{q}(x,\mu^2)=A'x^{\alpha'}(1-x)^{\beta'}. \tag{57}$$

The parametrization of the valence quarks is provided at the large scale $Q^2=10$ GeV$^2$, and its form at $Q^2=\mu^2$ is obtained from backward QCD evolution. Parameters describing the parton distributions come from a fit to the data at large $Q^2$ and are also constrained by the sum rules. As a result of the QCD evolution, the gluon and sea-quark distributions (multiplied by $x$) become singular at small $x$ for $Q^2>\mu^2$. In the leading-twist approximation the absolute value of the slope in $x$ of these distributions, and so the absolute value of the slope in $x$ of the $F_2$, grows with increasing $Q^2$. Naturally the model, which is based on perturbative QCD, cannot be extended into the region of $Q^2\leqslant\Lambda^2$ ($\Lambda$ is the QCD scale parameter), since the (perturbatively calculated) QCD coupling $\alpha_s(Q^2)$ diverges for $Q^2\to\Lambda^2$. Moreover, measurable quantities like the $F_2$ may contain non-negligible higher-twist contributions in the region of moderately small $Q^2$ [see Eq. (12)]. Presence of higher twists in an observable should not affect the QCD evolution of the leading-twist parton distribution, since partonic distributions of different twists evolve separately. Surprisingly, the QCD evolution turns out to be stable, and gives positive-definite parton distributions down to the very small scale $Q^2\cong(2\Lambda)^2$. Also it turns out that in the next-to-leading order approximation of perturbative QCD, $F_2$ is more stable than the distributions of partons (Glück and Reya, 1993). Although the higher-twist contribution can in principle be important in the low-$Q^2$ region, the leading-twist $F_2$ calculated within the model has recently been confronted successfully (Glück, Reya, and Vogt, 1995) with the low-$x$, low- and moderate-$Q^2$ NMC and E665 data (Fig. 6). The low-$x$ results of HERA, at slightly higher $Q^2$, are reasonably described as well (see Fig. 21).

The explicit forms of the parton distributions' parametrizations are as follows:

$$xv(x,Q^2)=Nx^a(1+A\sqrt{x}+Bx)(1-x)^D \tag{58}$$

for valence quarks;

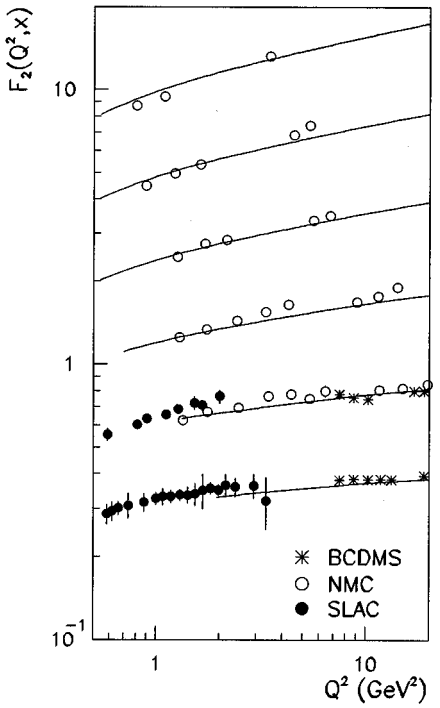


FIG. 7. Parametrization of $F_2^p(x,Q^2)$ by Badełek and Kwieciński as a function of $Q^2$ for the following values of $x$ (from the top): 0.008, 0.0125, 0.0175, 0.035, 0.07, and 0.1, together with data from the NMC (Amaudruz *et al.*, 1992b, 1992c). SLAC (Whitlow, Riordan, Dasu, Rock, and Bodek, 1992), and BCDMS (Benvenuti *et al.*, 1989, 1990). The $F_2$ values are scaled for clarity by the factors (from the top) 32, 26, 8, 4, 2 and 1. The error bars represent statistical and systematic errors added in quadrature. From Badełek, Bentvelsen, Kooijman, Kwieciński, Spiesberger, and von Schlippe, 1993.

$$xw(x,Q^2)=\left[x^a(A+Bx+Cx^2)\left(\ln\frac{1}{x}\right)^b + s^\alpha\exp\left(-E+\sqrt{E's^\beta\ln\frac{1}{x}}\right)\right](1-x)^D \quad (59)$$

for gluon and light sea-quarks; and

$$xw'(x,Q^2)=\frac{(s-s_{w'})^\alpha}{\left(\ln\frac{1}{x}\right)^a}(1+A\sqrt{x}+Bx)(1-x)^D \times\exp\left(-E+\sqrt{E's^\beta\ln\frac{1}{x}}\right) \quad (60)$$

for heavy sea-quarks, where $s$ in the formulas (59)–(60) is

$$s=\ln\frac{\ln[Q^2/\Lambda^2]}{\ln[\mu^2/\Lambda^2]}. \quad (61)$$

In these equations $A$, $B$, $C$, $D$, $E$, $E'$, $a$, and $b$ are low-order polynomials in $s$. These polynomials as well as values for the remaining parameters can be found in Glück, Reya, and Vogt (1992, 1995).

An electroproduction structure function $F_2$ for the low-$Q^2$, low-$x$ region was developed by Badełek and Kwieciński (Kwieciński and Badełek, 1989; Badełek and Kwieciński, 1992). Contributions from both the parton model with QCD corrections suitably extended to the low-$Q^2$ region and from the low-mass vector mesons were taken into account. The former contributions result from a large-$Q^2$ structure-function analysis (Roberts, 1992; Martin, Stirling, and Roberts, 1993a, 1993b) that includes the recent $F_2$ measurements of the NMC (Amaudruz *et al.*, 1992b, 1992c).

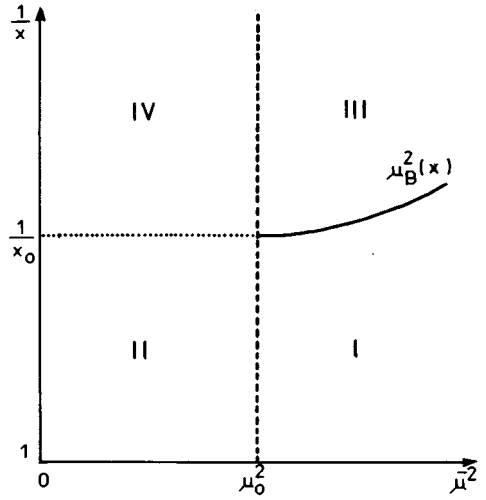


FIG. 8. Regions of the $(x,\mu^2)$ plane as used in the parametrization of Schuler and Sjöstrand. From Schuler and Sjöstrand, 1993.

The starting point is the generalized VMD representation of the structure function $F_2(x,Q^2)$ (Kwieciński and Badełek, 1989):

$$F_2[x=Q^2/(s+Q^2-M^2),Q^2] = \frac{Q^2}{4\pi}\sum_v \frac{M_v^4\sigma_v(s)}{\gamma_v^2(Q^2+M_v^2)^2}+Q^2\int_{Q_0^2}^\infty dQ'^2\frac{\Phi(Q'^2,s)}{(Q'^2+Q^2)^2} \equiv F_2^{(v)}(x,Q^2)+F_2^{(p)}(x,Q^2). \quad (62)$$

The function $\Phi(Q^2,s)$ is expressed as follows:

$$\Phi(Q^2,s)=-\frac{1}{\pi}\mathrm{Im}\int^{-Q^2}\frac{dQ'^2}{Q'^2}F_2^{\mathrm{AS}}(x',Q'^2). \quad (63)$$

The asymptotic structure function $F_2^{\mathrm{AS}}(x,Q^2)$ is assumed to be given. It may be obtained from the QCD structure-function analysis in the large-$Q^2$ region. By construction, $F_2(x,Q^2)\to F_2^{\mathrm{AS}}(x,Q^2)$ for large $Q^2$. The second term in (62) can be looked upon as the extrapolation of the (QCD-improved) parton model to arbitrary $Q^2$. The first term corresponds to the low-mass vector-meson dominance part, since the sum extends over the low-mass vector mesons. The contribution of vector mesons heavier than $Q_0$ is included in the integral in (62). Choosing the parameter $Q_0^2>(M_v^2)_{\max}$, where $(M_v)_{\max}$ is the mass of the heaviest vector meson included in the sum, one explicitly avoids double counting when adding the two separate contributions to the struc-

ture function. Note that $Q_0$ should be smaller than the mass of the lightest vector meson not included in the sum. The representation (62) is written for fixed $s$ and is expected to be valid for $s \gg Q^2$, i.e., at low $x$ but for arbitrary $Q^2$.

In Badełek and Kwieciński (1992), the representation (62) for the partonic part $F_2^{(p)}(x,Q^2)$ was simplified as follows:

$$F_2^{(p)}(x,Q^2)=\frac{Q^2}{(Q^2+Q_0^2)}F_2^{\mathrm{AS}}(\bar{x},Q^2+Q_0^2), \tag{64}$$

where

$$\bar{x}=\frac{Q^2+Q_0^2}{s+Q^2-M^2+Q_0^2}\equiv\frac{Q^2+Q_0^2}{2M\nu+Q_0^2}. \tag{65}$$

The simplified parametrization (64) connecting $F_2^{(p)}(x,Q^2)$ to $F_2^{\mathrm{AS}}$ by an appropriate change of the arguments of the latter possesses all the main properties of the second term in Eq. (62). First of all, it is evident that $F_2^{(p)}(x,Q^2)\to F_2^{\mathrm{AS}}(x,Q^2)$ for large $Q^2$. Moreover, the parametrization of $F_2^{(p)}$ defined by Eq. (64) preserves the analytic properties of the second term in Eq. (62).

It should be stressed that, apart from the parameter $Q_0^2$ which is constrained by the physical requirements described above, the representation (62) does not contain any free parameters, except of course those which are implicitly present in the parametrization of parton distributions defining $F_2^{\mathrm{AS}}$.

The proton structure function $F_2^p$ calculated from the representation (62) with $F_2^{(p)}(x,Q^2)$ given by Eq. (64) is shown in Fig. 7. In the "approach to scaling" (i.e., in the $Q^2$ dependence of $F_2$ at $Q^2$ less than 1 GeV$^2$ or so) visible in Fig. 7, the change of curvature comes from the factor $Q^2$ in Eq. (62), and the magnitude of this change, particularly at $Q^2 \ll 1$ GeV$^2$, is controlled by the vector-meson contribution, a nontrivial test of this mechanism. Although the vector-meson contribution $F_2^{(v)}$ dominates in the very-low-$Q^2$ region ($Q^2<1$ GeV$^2$), the partonic component $F_2^{(p)}$ still gives a significant contribution (i.e., at least 20–30 %). At $Q^2=10$ GeV$^2$ the structure function $F_2$ calculated from the model differs from $F_2^{\mathrm{AS}}(x,Q^2)$ by less than 3%. In the fixed-target energy range the model overestimates the magnitude of the total photoproduction cross section by 10–15 %.

The $x$ dependence at fixed $Q^2$ reflects both the energy-dependence of $\sigma_v$ and the $x$-dependence of $F_2^{\mathrm{AS}}$. Expectations coming from Regge theory are incorporated in the parametrizations of the $\sigma_v(s)$ (Kwieciński and Badełek, 1989) and of the input parton distributions at the reference scale $Q^2=4$ GeV$^2$ (Martin, Stirling, and Roberts, 1993a, 1993b). $F_2(x,Q^2)$ increases with decreasing $x$, which reflects the increase of the total cross sections $\sigma_v(s)$ with increasing $s$ as well as the increase of $F_2^{(p)}(x,Q^2)$ with decreasing $x$. The increase of $F_2^{(p)}(x,Q^2)$ with decreasing $x$ is weaker at small $Q^2$ than the similar increase in the large-$Q^2$ region. The $s$ dependence of $\sigma_v(s)$ is also relatively weak in the relevant region of $s$ (Kwieciński and Badełek, 1989). As a result the $x$ dependence of $F_2(x,Q^2)$ is relatively weak for low $Q^2$.

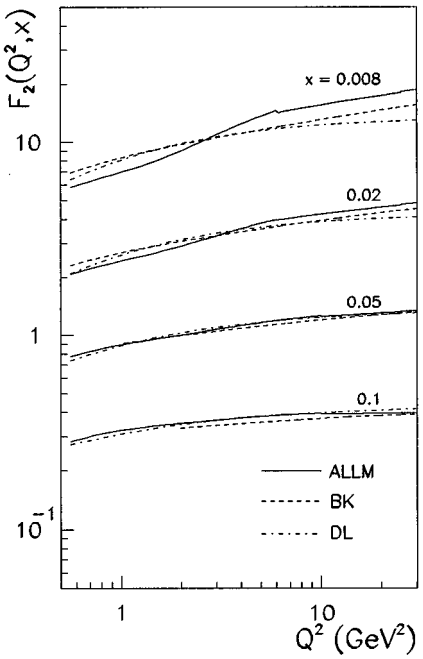


FIG. 9. Comparison of the parametrizations of $F_2^p(x,Q^2)$ by Abramowicz *et al.* (full curves), Badełek and Kwieciński (dashed curves), and Donnachie and Landshoff (dash-dotted curves) as functions of $Q^2$ for the following values of $x$ (from the top): 0.008, 0.02, 0.05, and 0.1. The values are scaled for clarity by the factors (from the top) 27, 9, 3, and 1. From Badełek, Bentvelsen, Kooijman, Kwieciński, Spiesberger, and von Schlippe, 1993.

The model is applicable in the small-$x$ region ($x<0.1$) and for arbitrary $Q^2$; however, its way of parametrizing the total vector-meson–nucleon cross sections imposes an additional constraint: $\nu>10$ GeV. The structure function $F_2(x,Q^2)$ calculated from the model is used in radiative-corrections calculations in deep-inelastic scattering experiments by, among others, the NMC and SMC at CERN.

The parametrization of Schuler and Sjöstrand (Schuler and Sjöstrand, 1993) extends those of Abramowicz *et al.* and Donnachie and Landshoff by explicitly including the damping of structure functions at small $x$, which is implied by screening effects in QCD (Gribov, Levin, and Ryskin, 1983; Levin and Ryskin, 1990), and by taking into account logarithmic scaling violations at large $Q^2$. Extrapolations towards the region of small $Q^2$ are carried out using the same damping factors as in Donnachie and Landshoff (1984, 1994) and Abramowicz, Levin, Levy, and Maor (1991). In the region of low $x$ the Regge parametrization is used. In practice the $(x,\mu^2)$ plane ($\mu^2=Q^2$) is divided into four regions, as shown in Fig. 8, and a different parametrization of parton distributions is assumed in each region. For large $\mu^2$ ($\mu^2>\mu_0^2$) the regions of large and small $x$ (regions I and III in Fig. 8) are divided by the boundary curve $\mu_B^2(x)$, given by

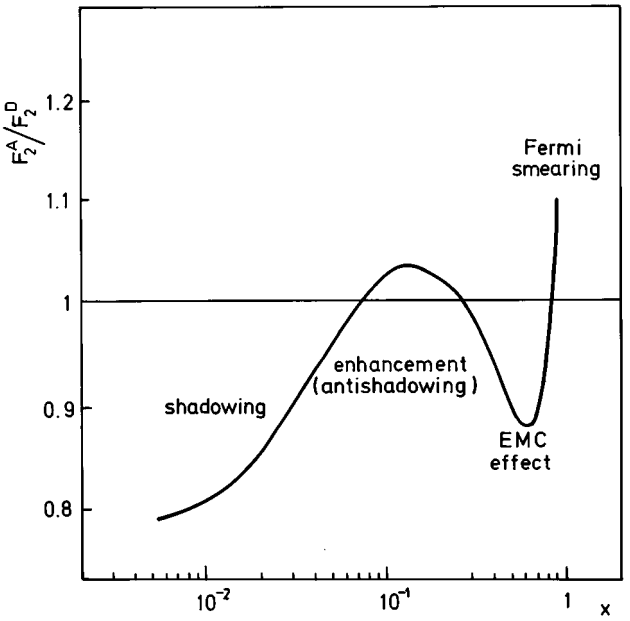


FIG. 10. Sketch of the $x$ dependence of the ratio $F_2^A/F_2^d$ indicating various nuclear effects.

$$\mu_B^2(x)=2+0.053^2\exp\left(3.56\sqrt{\ln\frac{1}{3x}}\right). \tag{66}$$

In the region I of large $\mu^2$ and large $x$, the structure function $F_2$ is given by the QCD-improved parton model with scale-dependent quark distributions $f_{v,s}(x,\mu^2)$, where the subscripts $v$ and $s$ denote the valence and sea distributions. The distributions $f_{v,s}(x,\mu^2)$ satisfy the Altarelli-Parisi evolution equations. In the regions II–IV the structure function $F_2$ is again expressed in terms of the quark distributions $\hat{f}_{v,s}(x,\mu^2)$, with their $\mu^2$ dependence being different in different regions. In the region II of small $\mu^2$ and large $x$ $(x>x_0)$, the structure functions are damped by the $\mu^2$-dependent factors, and valence distributions are made harder, i.e.,

$$\hat{f}_v(x,\mu^2)=\left(\frac{\mu^2}{\mu_0^2}\frac{\mu_0^2+m_R^2}{\mu^2+m_R^2}\right)^{(1-\eta)(1-x)/(1-x_0)} f_v(x,\mu_0^2), \tag{67}$$

$$\hat{f}_s(x,\mu^2)=\left(\frac{\mu^2}{\mu_0^2}\frac{\mu_0^2+m_P^2}{\mu^2+m_P^2}\right)^{1+\epsilon} f_s(x,\mu_0^2). \tag{68}$$

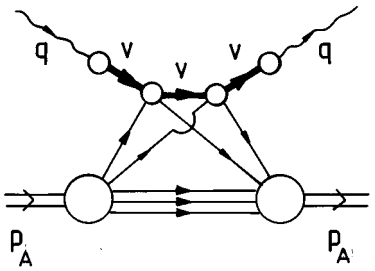


FIG. 11. Multiple scattering of vector mesons. Lines in the lower part of the diagram denote nucleons.

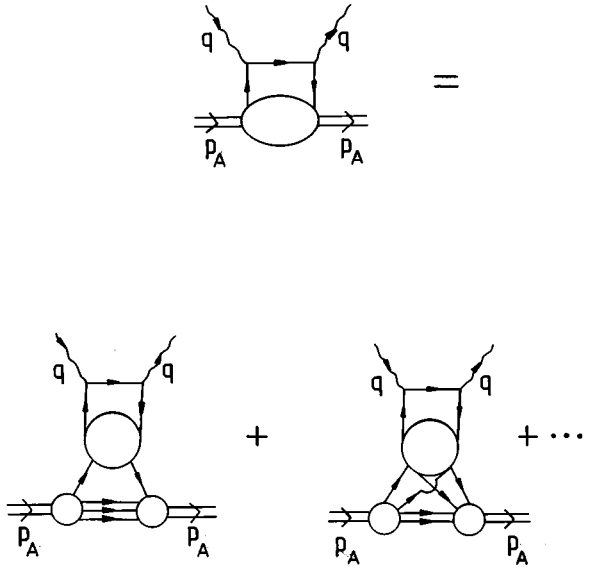


FIG. 12. Handbag diagram for virtual Compton scattering on a nucleus and its decomposition into a multiple-scattering series. Lines in the upper parts of diagrams denote quarks (antiquarks) and lines in the lower parts denote nucleons.

In the region III of large $\mu^2$ $[\mu_0^2<\mu^2<\mu_B^2(x)]$ and small $x$, the sea and valence quark distributions are parametrized as follows:

$$x\hat{f}_v(x,\mu^2)=N_1\left(\frac{x}{x_0}\right)^{\eta} x_0 f_v(x_0,\mu_0^2)+N_2 x f_v(x,\mu_B^2(x)), \tag{69}$$

$$x\hat{f}_s(x,\mu^2)=N_1\left(\frac{x}{x_0}\right)^{-\epsilon} x_0 f_s(x_0,\mu_0^2) + N_2 x f_s(x,\mu_B^2(x)), \tag{70}$$

where

$$N_1=\frac{\ln(\mu_B^2/\mu^2)}{\ln(\mu_B^2/\mu_0^2)}, \tag{71}$$

$$N_2=1-N_1. \tag{72}$$

Finally, in the region IV of small $x$ and small $\mu^2$, the valence- and sea-quark distributions are parametrized in the Regge form with the appropriate damping factors which guarantee vanishing of the structure function $F_2$ in the limit $\mu^2=0$:

$$x\hat{f}_v(x,\mu^2)=\left(\frac{x}{x_0}\right)^{\eta}\left[N_1\left(\frac{\mu_0^2+\mu_R^2}{\mu_0^2}\right)^{1-\eta} x_0 f_v(x_0,\mu_0^2) + N_2 x_0^{\eta} N^v\right], \tag{73}$$

$$x\hat{f}_s(x,\mu^2)=\left(\frac{x}{x_0}\right)^{-\epsilon}\left[N_1\left(\frac{\mu_0^2+\mu_R^2}{\mu_0^2}\right)^{1+\epsilon} x_0 f_s(x_0,\mu_0^2) + N_2 x_0^{-\epsilon} N^s\right], \tag{74}$$

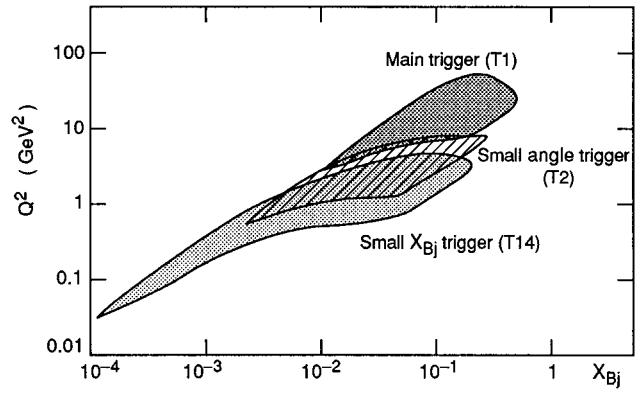


FIG. 13. Kinematic ranges covered by different triggers used by the NMC (Arneodo *et al.*, 1995b).

where now

$$N_1=1-\frac{x_0-x}{x_0}\frac{\mu_0^2-\mu^2}{\mu_0^2}, \tag{75}$$

$$N_2=1-N_1. \tag{76}$$

The parameters $\epsilon$ and $\eta$ correspond to the (effective) intercepts of the Pomeron and the Reggeon, respectively ($\epsilon=0.56$, $\eta=0.45$). The values of the remaining parameters appearing in the formulas (67)–(75) are as follows: $\mu_0^2=5$ GeV$^2$, $x_0=0.0069$, $m_R^2=0.92$ GeV$^2$, $m_P^2=0.38$ GeV$^2$, $N_d^v=0.121$, $N_u^v=2N_d^v$, $N_d^s=N_u^s=N_{\bar d}^s=N_{\bar u}^s=0.044$, and $N_s^s=N_{\bar s}^s=0.5N_d^s$. The structure function $F_2(x,Q^2)$ is expressed in terms of the quark (and antiquark) effective distribution functions $\hat f_i(x,Q^2)$ using the parton-model formula

$$F_2(x,Q^2)=x\sum_i e_i^2\hat f_i(x,Q^2). \tag{77}$$

The QCD structure-function analysis of Martin, Roberts, and Stirling (Martin, Stirling, and Roberts, 1993a, 1993b, 1994) has recently been extended to cover the region of low $Q^2$ (Martin, Stirling, and Roberts, 1995). It is based on the next-to-leading order approximation of QCD and on modifications of parton distributions by a form factor

$$\rho(x,Q^2)=\frac{Q^2}{Q^2+m^2} \tag{78}$$

with

$$m^2=m_0^2(x)\exp(-Q^2/Q_0^2). \tag{79}$$

The function $m_0^2(x)$ was assumed to have the form

$$m_0^2(x)=Ax^{-n} \tag{80}$$

and the parameters $A$, $n$, and $Q_0^2$ were fitted to the data. Target-mass corrections, important for large $x$ and moderate values of $Q^2$, were also included by using a target-mass variable $\xi$ (Rujula de, Georgi, and Politzer, 1977) instead of $x$. Here

$$\xi=\frac{2x}{1+r} \tag{81}$$

with

$$r^2=1+\frac{4M^2x^2}{Q^2} \tag{82}$$

and $M$ the target mass. Effective parton distributions $f_i(x,Q^2)$ were then related to the QCD-evolved parton distributions $f_i^{\rm MRS}(x,Q^2)$ by

$$f_i(x,Q^2)=\rho(x,Q^2)f_i^{\rm MRS}(\xi,Q^2). \tag{83}$$

The parton distributions $f_i^{\rm MRS}(x,Q^2)$ satisfy the Altarelli-Parisi evolution equations in the next-to-leading order approximation. The evolution was frozen at $Q^2=Q_c^2$ where $Q_c^2=0.625$ GeV$^2$, i.e., $f_i^{\rm MRS}(Q^2,x)=f_i^{\rm MRS}(Q_c^2,x)$ for $Q^2<Q_c^2$. The starting distributions at $Q^2=Q_0^2=4$ GeV$^2$ were parametrized as follows (Martin, Stirling, and Roberts, 1993a, 1993b, 1994):

$$\begin{aligned}
xu_v&=A_u x^{\eta_1}(1-x)^{\eta_2}(1+\epsilon_u\sqrt{x}+\gamma_u x),\\
xd_v&=A_d x^{\eta_3}(1-x)^{\eta_4}(1+\epsilon_d\sqrt{x}+\gamma_d x),\\
xS&=A_s x^{-\lambda}(1-x)^{\eta_S}(1+\eta_S\sqrt{x}+\gamma_S x),\\
xg&=A_g x^{-\lambda}(1-x)^{\eta_g}(1+\gamma_g x).
\end{aligned} \tag{84}$$

The flavor structure of the quark sea at $Q^2=Q_0^2$ was taken as

$$\begin{aligned}
2\bar u&=0.4(1-\delta)S-\Delta,\\
2\bar d&=0.4(1-\delta)S+\Delta,\\
2\bar s&=0.2(1-\delta)S,\\
2\bar c&=\delta S,
\end{aligned} \tag{85}$$

with

$$x\Delta=A_\Delta x^{\eta_\Delta}(1-x)^{\eta_S}(1+\gamma_\Delta x). \tag{86}$$

The parameters defining the parton distributions (and the parameter $\delta$) are obtained from a global fit to the available data on deep-inelastic lepton scattering and other hard processes (Martin, Stirling, and Roberts, 1993a, 1993b, 1994).

The form factor $\rho(x,Q^2)$ ensures the proper behavior of the structure function $F_2(x,Q^2)$ in the limit $Q^2\to 0$. Its form is meant to accommodate in an approximate way the parton shadowing effects, which slow down the increase of the parton distributions with decreasing $x$ (Badełek, Charchuła, Krawczyk, and Kwieciński, 1992). The exponent $n$ controlling the small-$x$ behavior of the function $m_0^2(x)$ [see Eq. (80)] is in fact found to be remarkably close in value to the parameter $\lambda$ controlling the small-$x$ behavior of the sea-quark and gluon distributions [Eq. (84)]. As a result (see Fig. 19) one obtains in an economical way a simultaneous description of the large-$Q^2$ HERA data, which shows significant increase with decreasing $x$, as well as the fixed-target, low-$Q^2$ data, for which this dependence is rather weak (see Sec.

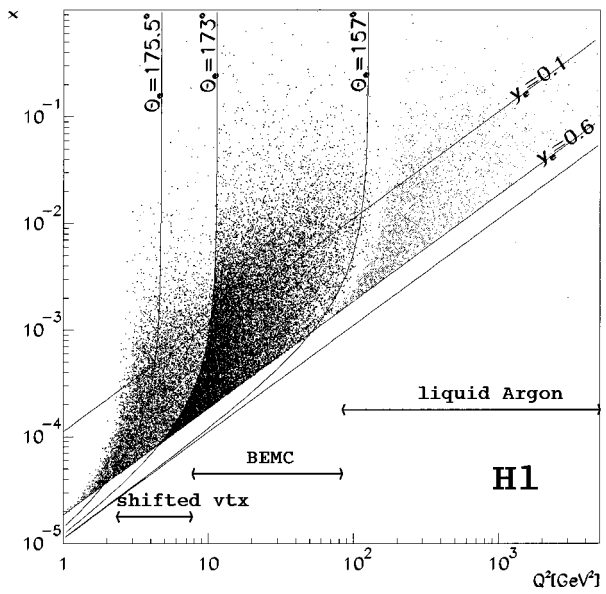


FIG. 14. Distribution of the neutral-current event sample in the $(x,Q^2)$ plane from the H1 experiment at HERA. The extension of the kinematic region by shifting the interaction vertex by 62 cm is also shown. Not marked are radiative events, which populate the region of lowest $Q^2$ and $x<10^{-3}$. From Eisele, 1995.

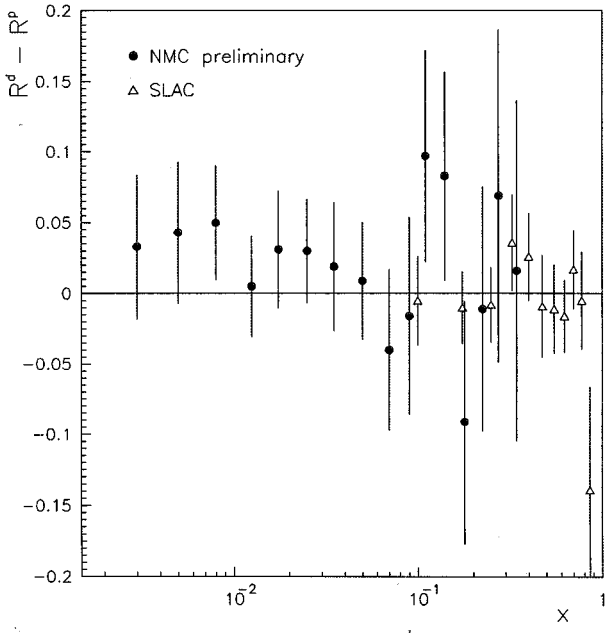


FIG. 15. NMC preliminary results for $R^d - R^p$ as a function of $x$ [see Granier, (NMC), 1994, for details] compared with the results of SLAC (open symbols; Whitlow, Rock, Bodek, Dasu, and Riordan, 1990). From Granier (NMC), 1994.

VIII). The resulting parametrization is applicable in the region $10^{-1}$ GeV$^2<Q^2<10^3$ GeV$^2$ and for arbitrary values of $x$.

Let us finally summarize the basic ingredients of the extrapolations of $F_2(x,Q^2)$ to low $Q^2$, discussed in Secs. V and VI. Most of the parametrizations essentially extend the parton-model formula for $F_2$ down to the low-$Q^2$ region, modifying the parton distributions in a suitable way; the model of Badełek and Kwieciński (Kwieciński and Badełek, 1989; Badełek and Kwieciński, 1992) also includes the VMD contribution along with the partonic one. The modifications are typically as follows:

(i) Instead of the variable $x$, modified variables $\bar{x}_i$ given by

$$\bar{x}_i = x\left(1+\frac{Q_{0i}^2}{Q^2}\right) \tag{87}$$

are used as arguments of the parton distributions, where $i$ labels the type of the parton. The variables $\bar{x}_i$ clearly approach $x$ for large $Q^2$, and become equal to $Q_{0i}^2/2M\nu$ at the photoproduction point, $Q^2=0$.

(ii) Models that at large $Q^2$ include the scaling violations implied by QCD either have the evolution in $Q^2$ frozen at scales below a certain scale $\bar{Q}_0^2$ (of the order of 1 GeV$^2$) or evolution in a shifted variable $Q^2+\bar{Q}_0^2$ is used.

(iii) Parton distribution functions are multiplied by form factors of the type $Q^2/(Q^2+m_i^2)$, which ensure vanishing of the structure function $F_2(x,Q^2)$ at $Q^2=0$.

Modifications are absent in the dynamical model of Glück, Reya, and Vogt (Glück, Reya, and Vogt, 1992,

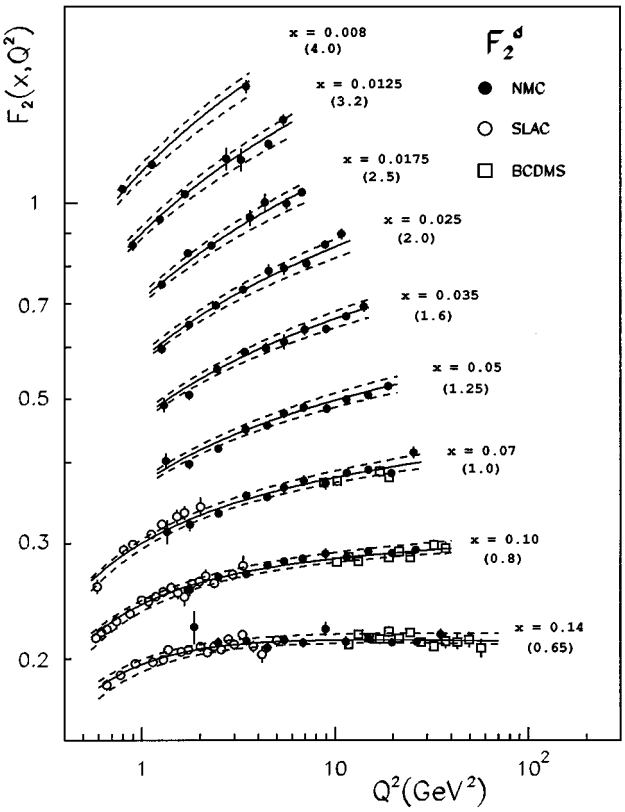


FIG. 16. The low-$x$ part of the $F_2^d$ data from the NMC (Arneodo *et al.*, 1995a) compared with the data from SLAC (Whitlow, Riordan, Dasu, Rock, and Bodek, 1992) and BCDMS (Benvenuti *et al.*, 1989, 1990). The error bars represent statistical errors. The solid curves are results of a 15-parameter function fit to all three data sets (see Table I). The detailed curves correspond to the extreme values of the parameters. From Arneodo *et al.*, 1995a.

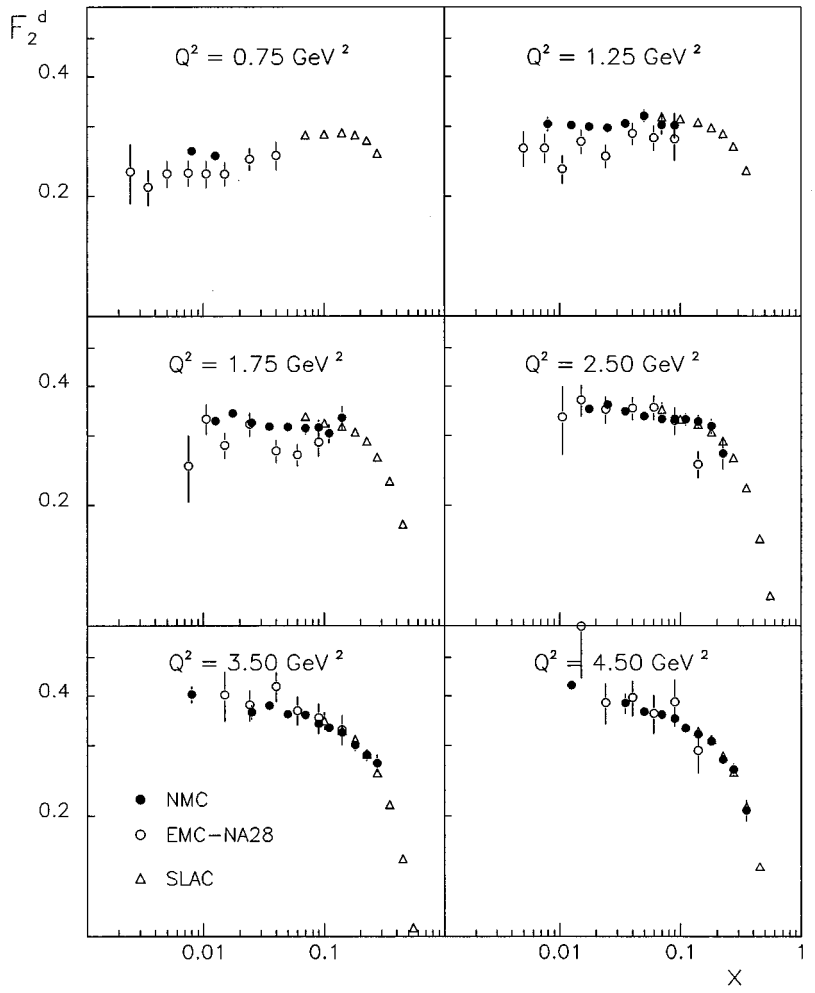


FIG. 17. Comparison of the low-$Q^2$ $x$ dependence of the NMC (Amaudruz *et al.*, 1992b, 1992c), EMC NA28 (Arneodo *et al.*, 1990), and SLAC (Whitlow, Riordan, Dasu, Rock, and Bodek, 1992) results. From Amaudruz *et al.*, 1992b, 1992c.

1993, 1995; Glück and Reya, 1993) which, in principle, is meant to describe the structure functions only in the large-$Q^2$ region, even if the QCD evolution is extended down to very low scales. Also the recent parametrization of the parton distributions by Martin, Stirling, and Roberts (1995) uses the variable $x$ instead of $\bar{x}$. This model does not, however, extend down to very low values of $Q^2$ ($Q^2<0.25$ GeV$^2$), and in particular, does not accommodate photoproduction.

The use of the variable $\bar{x}$ instead of $x$ in parametrizing the effective parton distributions is to a large extent pragmatic, since it makes possible a smooth transition to the photoproduction limit. In any case, at low $Q^2$ the variable $x$ is no longer representing the momentum fraction of the parent nucleon carried by a (probed) parton in the infinite-momentum frame. This may be seen by inspecting the kinematics of the virtual-photon—quark scattering [see Fig. 2(b)]. We introduce four-momenta $q'$ and $p'$ ( Landshoff, Polkinghorne, and Short, 1971) defined by

$$q'=q+xp,$$
$$p'=p-\frac{M}{2\nu}q, \tag{88}$$

and decompose the hit-quark four-momentum $k$ as follows:

$$k=\alpha p'-\beta q'+k_t, \tag{89}$$

where $k_t$ denotes the transverse momentum of the quark, orthogonal to both $p'$ and $q'$. Observe that $p'$ and $q'$ are approximately lightlike in the limit $\nu\to\infty$, $2M\nu\gg Q^2$, i.e., $p'^2=M^2/(4\nu^2)\approx 0$, $q'^2=x^2M^2\approx 0$. The parameter $\alpha$ has the meaning of the momentum fraction of a parent nucleon carried by a probed quark (antiquark) in the infinite-momentum frame. From the mass-shell condition $(k+q)^2=m_q^2$ ($m_q$ is a quark mass) we get

$$\alpha=x\left(1+\frac{k_t^2+m_q^2}{(1-\beta)Q^2}\right), \tag{90}$$

and find that the second term in (90) cannot be neglected at low $Q^2$.

It should also be remembered that the parton model itself is not justified at low $Q^2$. The effective "parton distributions" should therefore be regarded only as a way of parametrizing the structure functions. They cannot be treated as intrinsic properties that can be measured in a variety of processes, as is the case in the large-$Q^2$ limit. Moreover, the modifications (i)–(iii) explicitly introduce higher-twist corrections which go beyond the simple model of noninteracting partons.

Parametrizations of $F_2(x,Q^2)$ differ in their small-$x$ behavior. Most of them [except those of Donnachie and

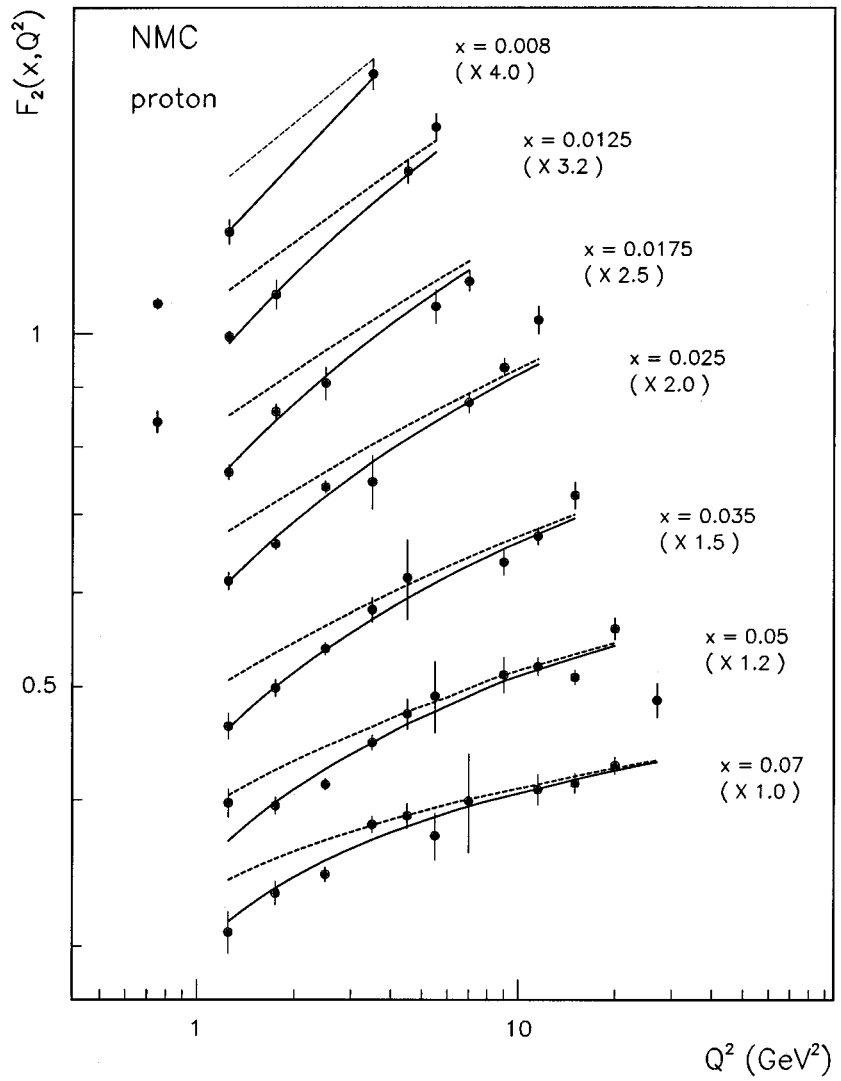


FIG. 18. The low-$x$ part of the results of the QCD fit to the $F_2^p$ data. The solid lines are the result of the QCD fit with higher twists included [see Eq. (15)]. The dotted curves show the contribution of $F_2^{\mathrm{LT}}$. In the fit, 90 (280) GeV data were renormalized by 0.993 (1.011). The errors are statistical. From Arneodo *et al.* (NMC), 1993.

Landshoff (Donnachie and Landshoff, 1984, 1994) and of the NMC (Amaudruz *et al.*, 1992d)] incorporate at large $Q^2$ the steep rise of $F_2(x,Q^2)$ with decreasing $x$, which is much stronger than implied (for instance) by expectations based on the soft Pomeron with intercept $\alpha_P=1.08$. This steep increase of $F_2(x,Q^2)$ with decreasing $x$ becomes very weak at low $Q^2$. The dynamical origin of this effect is different in different models, being attributed either to absorptive effects (Schuler and Sjöstrand, 1993; Capella, Kaidalov, Merino, and Trân Thanh Vân, 1994; Merino, 1994; Martin, Stirling, and Roberts, 1995), to the onset of the VMD mechanism (Kwieciński and Badełek, 1989; Badełek and Kwieciński, 1992), or to pure perturbative QCD effects related to the change in "evolution length" (Glück, Reya, and Vogt, 1992, 1993, 1995; Glück and Reya, 1993).

The summary above shows clearly that all attempts to describe the low-$Q^2$ region have their deficiencies, and it is thus difficult to recommend a particular one for practical use, e.g., in radiative corrections. Variations in the predictions obtained using different parametrizations may indicate the magnitude of systematic errors due to uncertainties in the input information to the radiative-correction calculations. It should be remembered, however, that those parametrizations that do not respect the kinematical constraint of Eq. (5) cannot be extended down to arbitrarily small values of $Q^2$, and so they cannot be used if this extension is required. Another shortcoming of certain parametrizations is their limitation in describing the change in the $x$ dependence of $F_2(x,Q^2)$ with $Q^2$ which is observed in the data. Finally, we would like to point out that parametrizations are being updated and developed as new experimental results appear.

A comparison of certain structure-function parametrizations is shown in Fig. 9 (see also Figs. 19 and 21). At the lowest measured values of $Q^2$ and $x$ none of the curves describes the data in a satisfactory way.

## VII. NUCLEAR SHADOWING

Nuclear effects in deep-inelastic lepton scattering may be inferred experimentally by inspecting the ratio $F_2^A/F_2^d$. In this method one tacitly assumes that the nuclear effects in $F_2^d$ can be neglected, or that $F_2^d=F_2^N$,

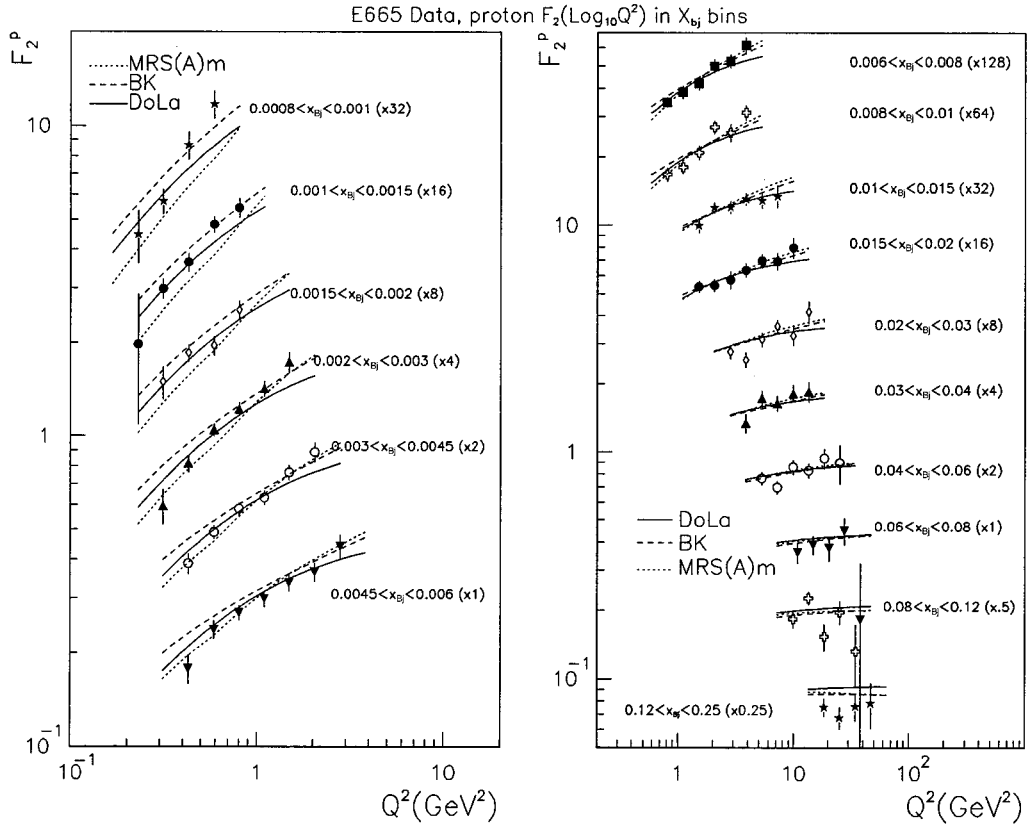


FIG. 19. Measurements of $F_2^p$ as a function of $Q^2$ in bins of $x$ by the E665 Collaboration at Fermilab. The errors bars are statistical and systematic uncertainties added in quadrature, but the normalization uncertainty (1.8%) is not included. Curves show model calculations of Martin, Stirling, and Roberts (1995), Badełek and Kwieciński (Kwieciński and Badełek, 1989; Badełek and Kwieciński, 1992), and Donnachie and Landshoff (1994). From Kotwal *et al.* (E665 Collaboration), 1995; Kotwal, 1995.

where $F_2^N$ decreases a free nucleon. In particular, nuclear shadowing corresponds to the $F_2^A/F_2^d$ ratio being smaller than unity at small $x$. In this sense shadowing can be regarded as part of the so-called EMC effect, as illustrated in Fig. 10.

Nuclear shadowing is a firmly established experimental fact (see Sec. VIII) which has been observed both in the low-$Q^2$ (including the photoproduction, i.e., $Q^2=0$) and in the large-$Q^2$ region. The nuclear structure function $F_2^A$ is then

$$F_2^A = F_2^N - \delta F_2^A , \tag{91}$$

where $\delta F_2^A$ denotes the shadowing term ($\delta F_2^A > 0$).

In the region of low $Q^2$ (and for photoproduction) the natural, and presumably the dominant, mechanism of nuclear shadowing is multiple scattering of vector mesons in the nucleus (Fig. 11). The vector mesons couple to virtual (or real) photons. This model gives the following contribution of shadowing to the nuclear structure function:

$$\delta F_2^A = \frac{Q^2}{4\pi} \sum_v \frac{M_v^4 \delta\sigma_v^A}{\gamma_v^2 (Q^2+M_v^2)^2}, \tag{92}$$

where the cross section $\delta\sigma_v^A$ is that part of the vector-meson–nucleus total cross section $\sigma_v^A$ (normalized to a nucleon) that corresponds to multiple scattering, i.e.,

$$\sigma_v^A = \sigma_v^N - \delta\sigma_v^A . \tag{93}$$

Here $\sigma_v^N$ is the vector-meson—nucleon total cross section, and the remaining quantities in the formula (92) are defined in Sec. III. The cross section that corresponds to multiple scattering can be obtained from the Glauber theory (Glauber, 1959; Bauer, Spital, Yennie, and Pipkin, 1978). The negative sign in Eq. (93) reflects the fact that the vector-meson–nucleon scattering amplitude is assumed to be imaginary. Thus in the VMD model, the shadowing in inelastic lepton-nucleus scattering reflects the absorptive character of the elementary vector-meson–nucleon scattering amplitude. It follows from Eq. (92) that the shadowing term corresponding to multiple rescaling of (a finite number of) vector mesons vanishes for large $Q^2$.

At large $Q^2$ one expects the parton model to be applicable. This leads to Bjorken scaling mildly violated by perturbative QCD corrections. The parton model is described by the "handbag" diagram of Fig. 12. It is this handbag structure, and the pointlike coupling of the photons to partons (i.e., to quarks and antiquarks), that guarantees the Bjorken scaling (modulo perturbative QCD corrections) independently of the structure of the lower part of the diagram. Nuclear shadowing in the large-$Q^2$ region may come from multiple-interaction contributions to the lower part of the handbag diagram,

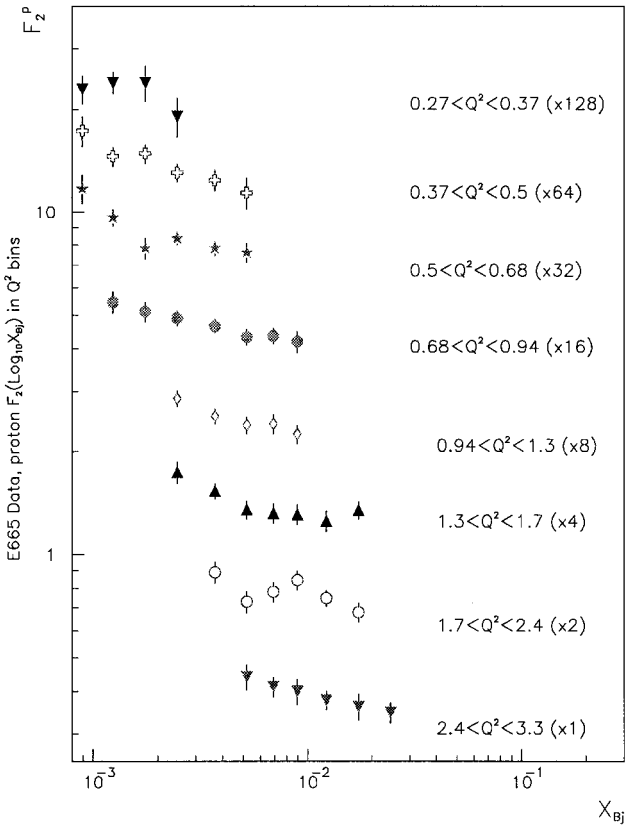


FIG. 20. As in Fig. 19, but $F_2^p$ is shown as a function of $x$ in bins of $Q^2$.

as shown in Fig. 12. Different models of shadowing correspond to different structural details of the diagrams of Fig. 12 (see Arneodo, 1994).

Shadowing is expected to be a low-$x$ phenomenon. This can be understood within a simple space-time picture of the interaction of a virtual photon with an atomic nucleus (Dokshitzer, Khoze, Mueller, and Troyan, 1991). In the infinite-momentum frame, i.e., in a frame where the momentum $p=p_A/A$ is very large, the wee partons (sea quarks and gluons) occupy longitudinal distances

$$\Delta z_p \approx \frac{1}{xp}. \tag{94}$$

The momentum $p_A$ is the momentum of the nucleus with $A$ nucleons. The nucleus in this frame occupies the Lorentz-contracted distance

$$\Delta z_A \approx 2R_A \frac{M}{p}, \tag{95}$$

where $R_A$ is the nuclear radius and $M$ the nucleon mass. The (Lorentz-contracted) average distance between the nucleons in this frame is

$$\Delta z = r\frac{M}{p}, \tag{96}$$

where $r$ denotes the average distance between nucleons in the laboratory frame. One can distinguish the regions in $x$:

$$\text{(i)} \quad x > \frac{1}{Mr}, \tag{97}$$

corresponding to the partonic size being smaller than the average distance between nucleons within nuclei,

$$\Delta z_p < \Delta z. \tag{98}$$

In this region the shadowing is expected to be negligible, since partons can be regarded as belonging to individual nucleons.

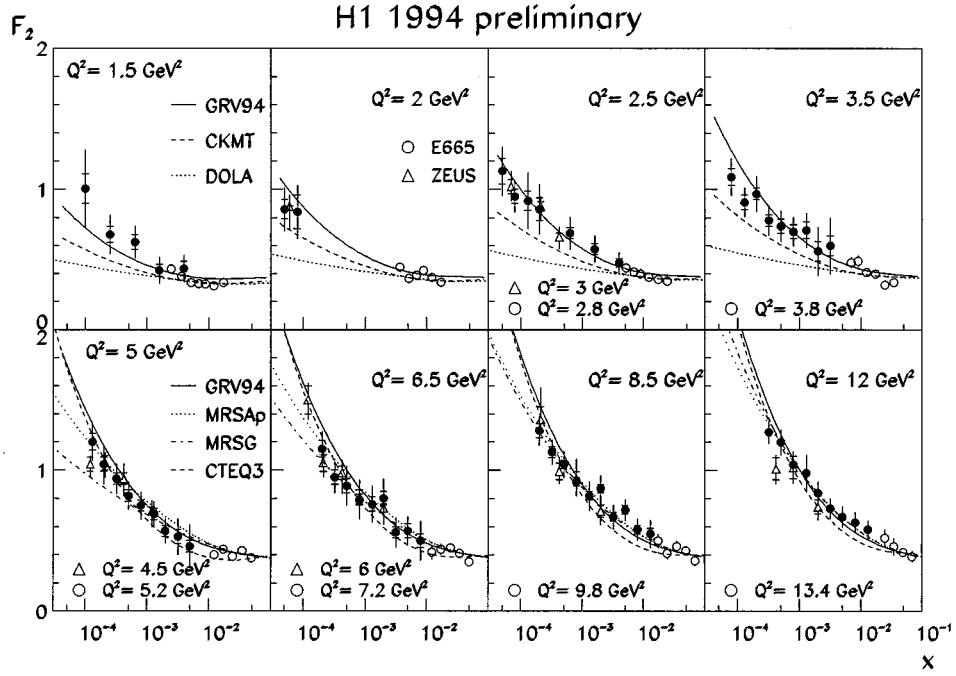


FIG. 21. Preliminary $F_2$ results at low $Q^2$ from the H1 experiment at HERA. The inner error bars mark statistical errors, the full bars represent statistical and systematic errors added in quadrature (excluding the systematic error in the luminosity). From Eisele, 1995.

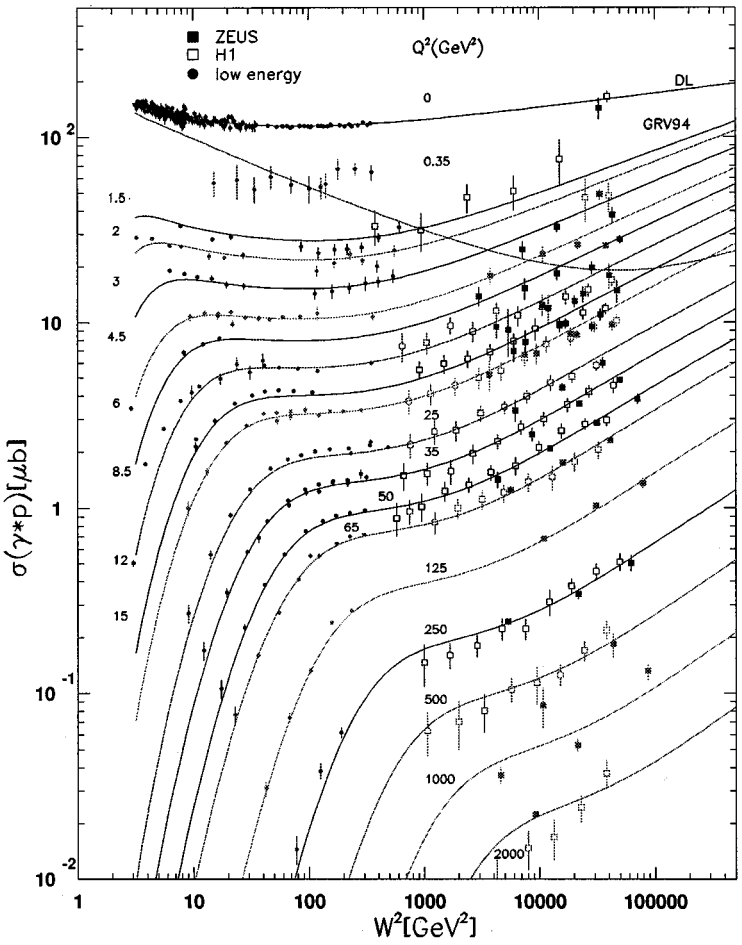


FIG. 22. The total virtual-photon cross section as a function of $W^2$ for different values of the photon virtuality $Q^2$. Curves are parametrizations of Donnachie and Landshoff (1994) and Glück, Reya, and Vogt (1995). In particular, the skewed curve is the Glück, Reya, and Vogt prediction for $Q^2=0.35$ GeV$^2$ (Levy, 1995a).

(ii) $$\frac{1}{2MR_A}<x<\frac{1}{Mr}, \tag{99}$$

corresponding to the longitudinal size of the partons being larger than the average distance between nucleons in a nucleus, yet smaller than the (contracted) longitudinal size of the nucleus:

$$\Delta z_A>\Delta z_p>\Delta z. \tag{100}$$

In this region the shadowing sets in gradually with decreasing $x$.

(iii) $$x<\frac{1}{2MR_A}, \tag{101}$$

corresponding to

$$\Delta z_p>\Delta z_A, \tag{102}$$

for which shadowing is expected to be maximal. In regions (i) and (ii) the partons can no longer be regarded as belonging to individual nucleons, since their longitudinal sizes are larger than the average distance between nucleons, and eventually exceed the size of the nucleus.

Let us also notice that when deep-inelastic scattering is considered in the laboratory frame, the three regions of $x$ are defined through the mutual relations between the lifetime $\tau_\gamma$ of the $q\bar{q}$ fluctuation of the virtual photon,

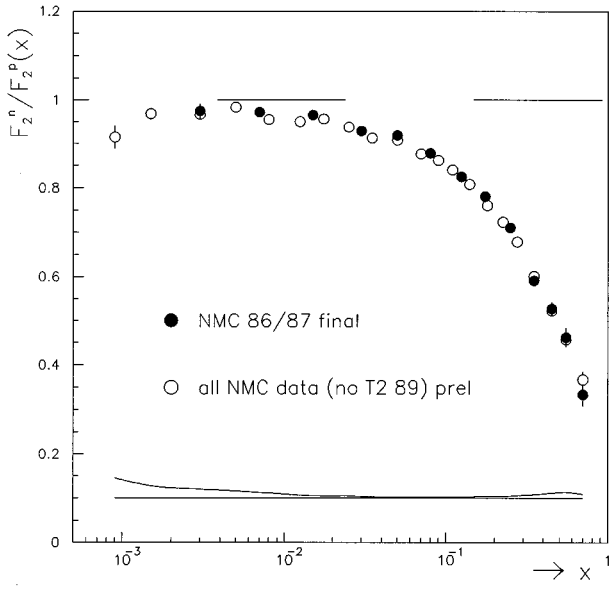


FIG. 23. NMC results on the ratio $F_2^n/F_2^p$ as a function of $x$ at $Q^2$ values averaged in each $x$ bin. The solid symbols mark the final data set [see Arneodo *et al.* (NMC), 1994] while the open ones are preliminary data taken with a special small-$x$ trigger. Errors are statistical; the band at the bottom indicates the preliminary estimate of systematic errors. From Dyring (NMC), 1994.

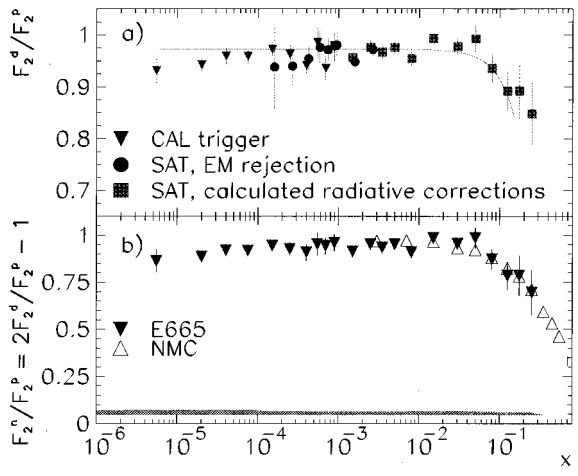


FIG. 24. E665 results. (a) $F_2^d/F_2^p$ as a function of $x$ for three different techniques of extracting the ratio. The curve shows a prediction of Badełek and Kwieciński (1994). (b) $2F_2^n/F_2^p=2F_2^d/F_2^p-1$ as a function of $x$. The NMC data at $Q^2=4$ GeV$^2$ (Arneodo *et al.*, 1994) are also shown. Errors are statistical. The systematic uncertainty is represented by the hatched area in part (b). From Adams *et al.* (E665 Collaboration), 1995b.

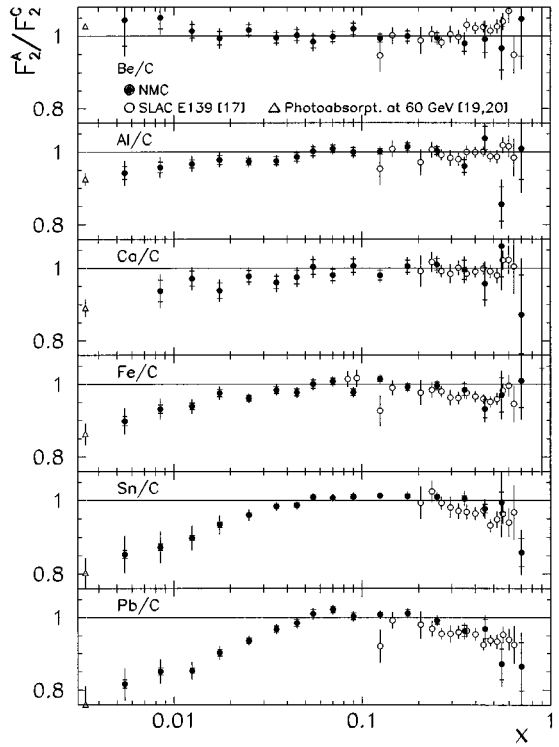


FIG. 25. NMC results on structure-function ratios $F_2^A/F_2^C$ as functions of $x$ averaged over $Q^2$ (open symbols), together with earlier results of SLAC [Arnold *et al.* (SLAC E139), 1984] (closed symbols). The inner error bars represent the statistical uncertainty, and the outer give statistical and systematic uncertainties added in quadrature. The SLAC E139 data for silver and gold were compared with NMC data for tin and lead, respectively. The photoabsorption cross-section data are given at a small value of $x$ for convenience. From Witzmann (NMC), 1995.

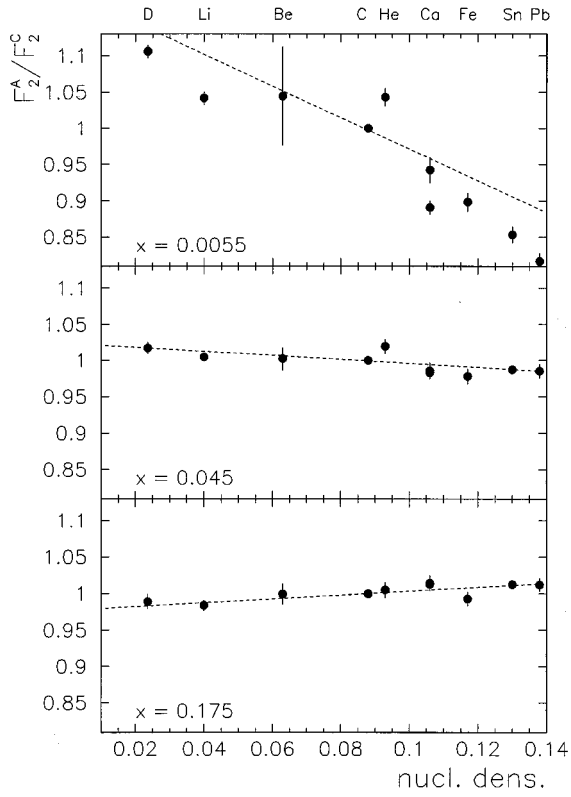


FIG. 26. Dependence on $A$ of the NMC $F_2^A/F_2^C$ data for three $x$ bins. Lines show the results of fits to the data with the function $F_2^A/F_2^C=cA^{(\alpha-1)}$. Errors are statistical. From Witzmann (NMC), 1995.

$$\tau_\gamma=\frac{1}{Mx}, \tag{103}$$

and the characteristic distances $r$ and $R_A$. Nuclear shadowing is indeed a typical small-$x$ phenomenon, since $1/(Mr)\approx 0.1$.

There exist several models of shadowing incorporating the VMD and/or the partonic mechanisms. For a complete review of these models and a comprehensive list of references, see Arneodo (1994). Since that article was completed, new papers concerning shadowing in the deuteron have appeared (Barone, Genovesse, Nikolaev, Predazzi, and Zakharov, 1993; Melnitchouk and Thomas, 1993a, 1993b; Badełek and Kwieciński, 1994),

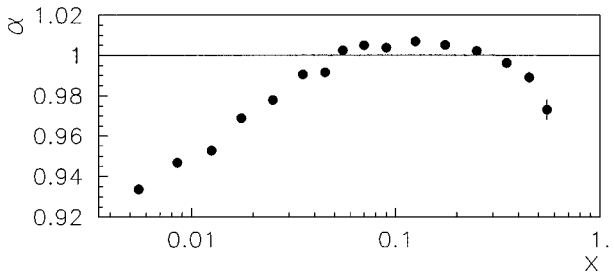


FIG. 27. Values of $\alpha$ from the $F_2^A/F_2^C=cA^{(\alpha-1)}$ fit to the NMC data [from Witzmann (NMC), 1995].

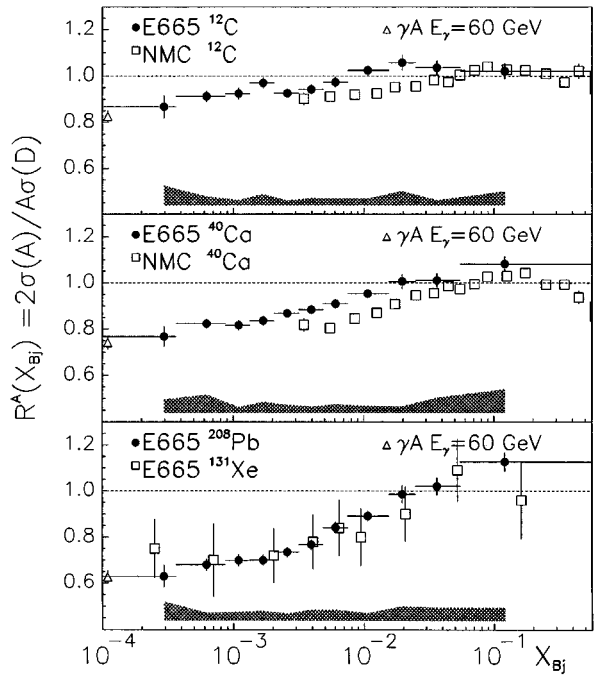


FIG. 28. E665 results on $\sigma^A/\sigma^D$ as a function of $x$. Errors are statistical, with systematic errors marked as shaded bands. The overall normalization uncertainties of 1.30%, 1.33%, and 1.55% (from top to bottom) have not been included. The NMC results have been shown for comparison where available. From Adams *et al.* (E665 Collaboration), 1995a.

several of them inspired by new measurements of the $F_2^d/F_2^p$ ratio (see Sec. VIII). Understanding shadowing effects in the deuteron has become relevant in view of the increased precision of measurements of the $F_2^A/F_2^d$ and $F_2^d/F_2^p$ ratios. In particular, the shadowing affects extraction of the neutron structure function from the data. This in turn affects (decreases) the magnitude of the experimentally evaluated Gottfried sum (Zoller, 1992a, 1992b; Badełek and Kwieciński, 1994).

## VIII. EXPERIMENTAL DATA

The experimental problems connected with measuring and analyzing the low-$x$, low-$Q^2$ data are discussed in Badełek, Charchuła, Krawczyk, and Kwieciński (1992). That reference also lists the experiments, the then-available experimental results, and their interpretation. Here we limit ourselves to updating this information.

In fixed-target experiments the low-$x$ region is correlated with low-$Q^2$ values, as in Fig. 13 (Arneodo *et al.*, 1995b). The lowest values of $x$ to date were attained by the NMC at CERN and the E665 Collaboration at Fermilab using special experimental techniques permitting the measurement of muon scattering angles as small as 1 mrad [Seitz and Witzmann (NMC), 1993; Dyring (NMC), 1994; Adams *et al.* (E665 Collaboration), 1995b; Arneodo *et al.* (NMC), 1995b]. These "small-$x$ triggers" and special off-line selection methods were also effective against a background of muons scattered elastically from target atomic electrons; the corresponding peak occurs at $x = 0.000\,545$. Systematic errors in both experiments,

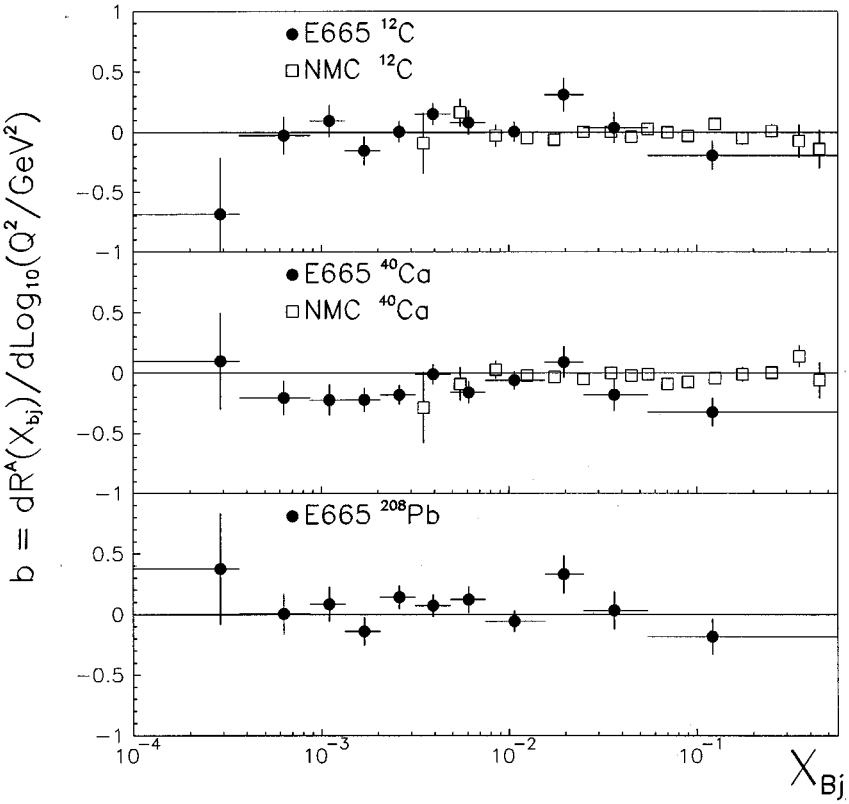


FIG. 29. $Q^2$ dependence of the E665 $F_2^A/F_2^D$ data in bins of $x$ (closed circles). Errors shown are the uncertainties resulting from the fit, in which only statistical errors were considered. The NMC results are shown as open squares. From Adams *et al.* (E665 Collaboration), 1995a.

and in particular errors in the ratio $F_2^a/F_2^b$ of structure functions for different nuclei, were greatly reduced by irradiating several target materials at a time and/or frequently exchanging targets in the beam.

At HERA the lowest values of $Q^2$ to date (1.5 or even 1 GeV$^2$ for the H1 and 2 GeV$^2$ for the ZEUS experiment) were attained recently by two methods: shifting the interaction point in the proton beam direction so as to increase the acceptance of low-$Q^2$ events (H1 and ZEUS) and using radiative events with hard-photon emission collinear with the incident electron (H1 only; lowest values of $Q^2$) (Fig. 14) (Eisele, 1995). The radiative events can be interpreted as nonradiative events with reduced electron-beam energy.

During the last three years new data on the proton and deuteron structure functions has emerged from the NMC (Amaudruz *et al.*, 1992b, 1992c; Arneodo *et al.*, 1995a), from the E665 Collaboration (Kotwal *et al.*, 1995; Kotwal, 1995), and from HERA (Eisele, 1995). Dedicated measurements of the ratio $F_2^d(x,Q^2)/F_2^p(x,Q^2)$ have also been performed both by the NMC (Arneodo *et al.*, 1994; Dyring, 1994) and by the E665 Collaboration (Adams *et al.*, 1993; Adams *et al.*, 1995b). The NMC also performed the QCD analysis of their $F_2$ data (Arneodo *et al.*, 1993). Both collaborations have presented new and precise results on the $x$, $A$, and $Q^2$ dependence of nuclear shadowing [Adams *et al.* (E665 Collaboration), 1992; Adams *et al.* (E665 Collaboration), 1995a; Amaudruz *et al.* (NMC), 1995; Arneodo *et al.* (NMC), 1995b; Witzmann (NMC), 1995]. The NMC also determined the differences $R^{Ca}-R^C$ (Amaudruz *et al.*, 1992a) and $R^d-R^p$ (Granier, 1994) at low $x$. A new measurement of $R(x,Q^2)$ has been reported by the NMC (Dyring, 1995) and by the CCFR Collaboration (Yang, 1995).

To extract $F_2(x,Q^2)$ from the data, one needs information on $R(x,Q^2)$. In particular, the ratio of inelastic cross sections on different nuclei is equal to the corresponding structure-function ratio, provided $R(x,Q^2)$ is the same for these nuclei. Results of the NMC analysis of $R^{Ca}-R^C$ and $R^d-R^p$ show that neither of these quantities exhibits a significant dependence on $x$, and that they are both consistent with zero (Fig. 15) (Granier, 1994). The NMC reported preliminary measurements of $R(x,Q^2)$ for the proton and deuteron as a function of $x$ in the range $0.006<x<0.14$ (Dyring, 1995). The average $Q^2$ of these measurements ranges from 1.1 GeV$^2$ at the smallest $x$ to 15.5 GeV$^2$ at $x=0.14$. The results show a rise of $R$ with decreasing (small) $x$. Preliminary measurements of $R(x,Q^2)$ on a heavy target, at $x>0.015$ and $Q^2>5$ GeV$^2$ (at present), have been reported recently by the CCFR neutrino collaboration [Yang (NMC), 1995]. In their data analyses, the NMC and the E665 Collaboration assumed $R$ to be independent of the target atomic mass $A$, and given by the SLAC parametrization (Whitlow, Rock, Bodek, Dasu, and Riordan, 1990), valid for $x>0.1$ and $Q^2>0.3$ GeV$^2$. This parametrization was then extrapolated (with 100% error) to $Q^2\to 0$. There is thus a need for a theoretical estimate of $R$ (or $F_L$) in the region of low $x$ and low $Q^2$. Two ongoing phenomenological studies are expected to deliver such estimates in the near future. Both the perturbative QCD contribution, which at low $x$ and low $Q^2$ is dominated by the photon-gluon mechanism, and a nonperturbative term are taken into account in these studies. In Badełek, Kwieciński, and Staśto (1996) the latter contribution is determined phenomenologically, while in Bodek and Yang (1995) it is fitted to the low-$Q^2$ data.

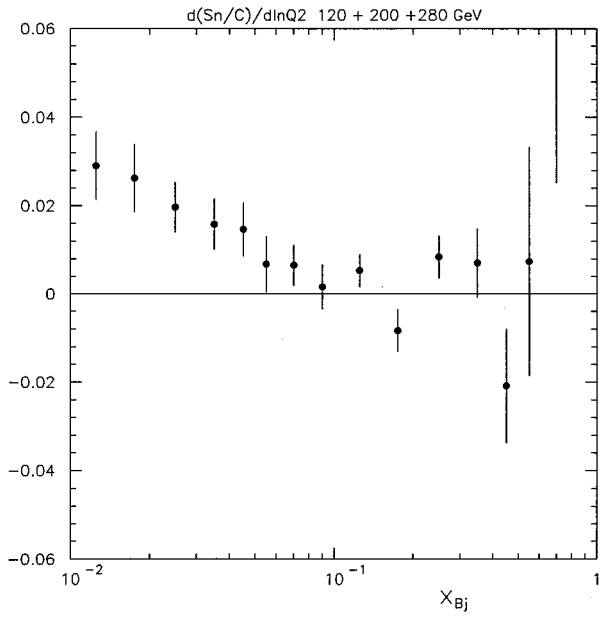


FIG. 30. $Q^2$ dependence of the preliminary NMC $F_2^{\mathrm{Sn}}/F_2^{\mathrm{C}}$ data in bins of $x$ (from Mücklich, 1995). Errors shown are the uncertainties resulting from the fit, in which only statistical errors were considered.

The NMC results for the proton and deuteron structure functions (Amaudruz *et al.*, 1992b, 1992c) cover the ranges $0.006\leqslant x\leqslant 0.6$ and $0.5\leqslant Q^2\leqslant 55$ GeV$^2$, and were the first precise measurements at such low values of $x$. These data had great impact on the parton distribution analysis (see, for example, Martin, Stirling, and Roberts, 1993a, 1993b), and joined well to the results of HERA (see below). In 1995 the NMC presented more complete results on $F_2^p$ and $F_2^d$ (Arneodo *et al.*, 1995a) (Fig. 16). A clear scaling violation pattern, with slopes $d\ln F_2/d\ln Q^2$ positive at low $x$, and an "approach to scaling" (i.e., $Q^2$ dependence of $F_2$ at $Q^2$ less than few GeV$^2$) are visible. In this figure, a comparison of the NMC, SLAC (Whitlow, Riordan, Dasu, Rock, and Bodek, 1992), and BCDMS Collaboration (Benvenuti *et al.*, 1989, 1990) measurements is also shown. All three data sets are in good agreement with one another. They were thus used to obtain parametrizations of $F_2^p$ and $F_2^d$ and their uncertainties (solid and dashed curves in Fig. 16, respectively), using the 15-parameter function, defined in Table I. At the same time, the low-$x$ results of the EMC NA2 (Aubert *et al.*, 1987) experiment have been disproved by the NMC measurements. The $x$ dependence of the deuteron structure function at low $Q^2$ is shown in Fig. 17 for several values of $Q^2$ (1992 data). The NMC measurements (Amaudruz *et al.*, 1992b, 1992c) are compared with

those of EMC NA28 (Arneodo *et al.*, 1990) and SLAC (Whitlow, Riordan, Dasu, Rock, and Bodek, 1992). Confirmed is a characteristic weak $x$ dependence of $F_2^d$ at low $Q^2$, observed for the first time by EMC NA28 (Arneodo *et al.*, 1990) and interpreted in Kwieciński and Badełek (1989) and Badełek and Kwieciński (1992) (see also Sec. VI).

The $Q^2$ dependence of the structure functions $F_2^p$ and $F_2^d$, measured by the NMC with good accuracy down to low values of $x$, has been compared with the predictions of perturbative QCD [Arneodo *et al.* (NMC), 1993]. The flavor singlet and nonsinglet quark distributions, as well as the gluon distribution, have been parametrized at a reference scale of 7 GeV$^2$. All the data with $Q^2 \geqslant 1$ GeV$^2$ were included in the fit. Along with the leading-twist contribution, the higher-twist term was also included in an approximate way given by formula (15), where $H(x)$ was determined from the SLAC and BCDMS measurements (Virchaux and Milsztajn, 1992) averaged over the proton and deuteron and suitably extrapolated to lower values of $x$. Results of the QCD fit to the proton structure-function data are shown in Fig. 18. Important here is the extension of the QCD analysis to the low-$x$ and low-$Q^2$ regions. The contribution of higher twists is still moderate at scales of about 1 GeV$^2$.

New measurements of the proton and deuteron structure functions for $x > 0.0001$ have been presented recently by the E665 Collaboration (Figs. 19 and 20) (Kotwal *et al.*, 1995; Kotwal, 1995). The lowest $Q^2$ values in their data reach 0.2 GeV$^2$, and the lowest $x$ are about $8 \times 10^{-4}$. A clear pattern emerges from these data at $Q^2$ values lower than a few GeV$^2$: weak $x$ and possibly stronger-than-logarithmic $Q^2$ dependence of $F_2$.

The E665 region of $x$, i.e., $x > 10^{-4}$, is now being investigated by both the H1 and ZEUS Collaborations at HERA. The most dramatic effect visible in their large-$Q^2$ data is a strong increase of $F_2$ with decreasing $x$. This complements the weak $x$ dependence of $F_2$ observed by EMC NA28, by the NMC, by the E665 Collaboration, and recently also by HERA (Fig. 21) in the low-$Q^2$ part of the small-$x$ region, as well as the rather weak increase of the photoproduction cross section with energy between fixed-target and HERA energies. The dynamics of the transition from high to low $Q^2$ is illustrated in a different way in Fig. 22 (Levy, 1995b).

Both the NMC and E665 experiments have measured the deuteron-to-proton structure-function ratio $F_2^d/F_2^p$ down to very low values of $x$. In case of the NMC the ratio was measured directly, i.e., the measurement of the absolute structure function is used only for the radiative-correction calculations. The data are usually presented as the ratio $F_2^n/F_2^p$, where $F_2^n$ is defined as $2F_2^d - F_2^p$. This quantity would give the structure function of the free nucleon in the absence of nuclear effects in the deuteron. The NMC results for $F_2^n/F_2^p$ as a function of $x$ are shown in Fig. 23 (Dyring, 1995); E665 results are presented in Fig. 24 (Adams *et al.*, 1995b). In both data sets the average $Q^2$ varies from bin to bin, reaching down to $\langle Q^2 \rangle = 0.2$ GeV$^2$ at $x = 0.0008$ for the NMC, and $\langle Q^2 \rangle = 0.004$ GeV$^2$ at $x = 5 \times 10^{-6}$ for E665. The results of both experiments show that $F_2^n/F_2^p$ always stays below unity down to the smallest measured values of $x$. At low $x$ this can be attributed to nuclear shadowing in the deuteron (Melnitchouk and Thomas, 1993a, 1993b; Badełek and Kwieciński, 1994; Barone, Genovesse, Nikolaev, Predazzi, and Zakharov, 1994), predicted to be only weakly $x$ dependent, as observed. That the results can also detect the difference in $F_2$ between protons and neutrons at low $x$ seems unlikely since, for example, in the Regge model the difference between the proton and neutron structure functions vanishes with decreasing $x$ (Zoller, 1992a, 1992b; Badełek and Kwieciński, 1994; Barone, Genovesse, Nikolaev, Predazzi, and Zakharov, 1994).

The NMC measurements of $F_2^D$ (fitted together with the SLAC and BCDMS data) and of $F_2^n/F_2^p$ allow the determination of the Gottfried sum $S_G = \int (F_2^p - F_2^n) dx/x$, with $F_2^p - F_2^n = 2F_2^d(1 - F_2^n/F_2^p)/(1 + F_2^n/F_2^p)$. At $Q^2 = 4$ GeV$^2$, with any $Q^2$ dependence neglected, $S_G$ was found to be $0.235 \pm 0.026$ [Arneodo *et al.* (NMC), 1994], significantly below the simple quark-parton model value of 1/3. Recently, non-negligible $Q^2$ dependence of $F_2^p - F_2^n$ as a function of $x$ for low $Q^2$ values has been reported: both the position of the maximum and the maximum value of this function change with $Q^2$. This change becomes negligible when higher-twist contributions of a form similar to Eq. (15) are separated out from the $F_2^d$ and $F_2^n/F_2^p$ measurements [Brüll (NMC), 1995].

New data have appeared on nuclear shadowing. Results of a high-precision study by the NMC of the $A$ dependence of nuclear shadowing in the range $0.004 < x < 0.6$ and 1.5 GeV$^2 < Q^2 < 60$ GeV$^2$ are shown in Figs. 25–27. The structure-function ratios $F_2^A/F_2^C$ for $A$=Be, Al, Ca, Fe, Sn, and Pb, in conjunction with earlier ones for $D$, He, Li, C, and Ca [Amaudruz *et al.* (NMC), 1995; Arneodo *et al.* (NMC), 1995b], together with earlier data from SLAC [Arnold *et al.* (SLAC E139), 1984], show in detail the $x$ dependence of shadowing (Fig. 23). The NMC data cover the $A$ range from $A = 2$ to $A = 208$. In Fig. 26, they are shown as a function of $A$ for three bins of $x$. The functional dependence of $F_2^A/F_2^C$ on $A$ has been parametrized as $F_2^A/F_2^C = cA^{(\alpha - 1)}$ in each bin of $x$. Values of the parameter $\alpha$ are displayed in Fig. 27. The amount of shadowing increases strongly with the mass number $A$. Much lower values of $x$ and $Q^2$ are covered by the nuclear data obtained by the E665 Collaboration: $x > 0.0001$ and $Q^2 > 0.1$ GeV$^2$ [Adams *et al.* (E665 Collaboration), 1995a], Fig. 28. However, the amount of shadowing observed by the E665 Collaboration, seems to be smaller than that measured by the NMC. Shadowing seems to saturate at $x$ about 0.004, as was observed earlier by the E665 Collaboration (Adams *et al.*, 1992 ), and as indicated by NMC data on the $F_2^{\mathrm{Li}}/F_2^D$ and $F_2^C/F_2^D$ ratios measured down to $x = 0.0001$ and $Q^2 = 0.03$ GeV$^2$ (Arneodo *et al.*, 1995b). No clear $Q^2$ dependence is visible

in the E665 data for a wide interval of $Q^2$ (Fig. 29), contrary to the preliminary NMC results in which a positive $Q^2$ slope for the ratio $F_2^{\mathrm{Sn}}/F_2^{\mathrm{C}}$ at $x<0.1$ is observed (Fig. 30) (Mücklich, 1995). The shadowing region seems to have another interesting feature: it contains a large fraction of wide-rapidity-gap (or diffractive) events, their fraction increasing with $A$ [Carroll (E665), 1995].

## IX. CONCLUSIONS AND OUTLOOK

In this review paper, we have summarized the present understanding of the electroproduction structure functions in the region of low values of $x$ and $Q^2$, which have recently been measured in fixed-target, charged-lepton inelastic-scattering experiments as well as at the HERA collider. This has included a survey of theoretical constraints and expectations, clarification of certain definitions and concepts, collection of the existing parametrizations of structure functions in this region, and presentation of the experimental data. We consider this paper to be an extension of the comprehensive review article on small-$x$ physics of Badełek, Charchuła, Krawczyk, and Kwieciński (1992) towards a more detailed treatment of the low-$Q^2$ problems. This means, in particular, that in the summary of experimental data we have presented only results that appeared after the above-mentioned article was completed.

An important property of the structure function $F_2(x,Q^2)$ that follows from conservation of the electromagnetic current is its linear vanishing as a function of $Q^2$ for $Q^2\to 0$ (for fixed $\nu$). This means that Bjorken scaling cannot be valid at low $Q^2$, so the pure partonic description of inelastic lepton scattering must break down for moderate and low $Q^2$ values. At moderately large $Q^2$ the higher-twist contributions to $F_2$, which vanish as negative powers of $Q^2$, are frequently being included in the QCD data analysis. One also expects that at low $Q^2$ the VMD mechanism should play an important role.

The small-$x$ behavior of the structure function $F_2(x,Q^2)$ is dominated by Pomeron exchange. Analysis of the structure function in the small-$x$ region for both low and moderate values of $Q^2$ can clarify issues connected with the Pomeron, including possible interplay between the soft and hard Pomerons, the role of shadowing (or absorptive) corrections, and so on. At large $Q^2$, the problem is linked with QCD expectations concerning deep-inelastic scattering at small $x$ (Kwieciński, 1993, 1994; Martin, 1994). Aside from the structure functions (or total cross sections), complementary information on the Pomeron can also be obtained from the analysis of diffractive processes in electro- and photoproduction. These include both inclusive diffractive processes and the diffractive production of vector mesons; the present experimental situation is described in Eisele (1995) and Levy (1995a).

Descriptions of the low-$Q^2$, low-$x$ behavior of $F_2$ range from pure fits to experimental data to the dynamically motivated models. The existing parametrizations have been collected in a way which should make them easy to use in practical applications, e.g., in the radiative-correction procedure. Wherever possible, the dynamical content of each parametrization was exposed.

Since 1992 a wealth of measurements of the nucleon structure function $F_2$ has been published. In the region of interest for this paper were the NMC and E665 results extending down to very low $x$ and $Q^2$ values and displaying characteristic "approach to scaling" behavior, as well as first results from HERA for $Q^2$ extending down to 1.5 $\mathrm{GeV}^2$. The data were analyzed using QCD, showing its applicability down to scales of the order of 1 $\mathrm{GeV}^2$. The nuclear shadowing phenomenon was studied in great detail for targets ranging from $A=2$ to $A=208$ by the NMC and the E665 Collaboration. Its $x$, $Q^2$, and $A$ dependences were measured precisely. Preliminary data on $R(x,Q^2)$ have also been reported.

The fixed-target (unpolarized) structure-function measurement program comes to an end in 1995. Many experiments (EMC, NMC, BCDMS, SLAC, CCFR) have contributed in this great and successful effort to learn about the properties of partons and strong interactions. Several aspects of this knowledge are not yet understood. One of these, and perhaps the most challenging, is low-$x$ dynamics and, in particular, its dependence on the probing photon virtuality, $Q^2$. New possibilities for the study of this problem have opened up with the advent of the HERA collider. The data collected there show a very strong increase of $F_2$ with decreasing $x$ at high $Q^2$. This increase becomes weaker at low $Q^2$, an effect known for a long time from fixed-target measurements and confirmed recently by low-$Q^2$ data from HERA. These data bridge the gap between the fixed-target and the collider low-$x$ results, opening up the possibility of a unified understanding of the underlying dynamics.

For fixed $Q^2$ the increase of the structure function $F_2(x,Q^2)$ with decreasing $x$ reflects the increase of the virtual Compton scattering total cross section with $W^2$. We would like to emphasize that this increase observed at large $Q^2$ is much stronger than the increase of the total photoproduction cross section observed between fixed-target and HERA energies. Dynamical understanding of this evident variation of the $W^2$ dependence with $Q^2$ is certainly very interesting and important. Experimental data at low values of $Q^2$ ($Q^2\simeq 1$ $\mathrm{GeV}^2$) covering a similar range of $W^2$ as those at high $Q^2$ would be extremely valuable for this purpose. It would therefore be very interesting to continue extending the HERA measurements down to lower values of $Q^2$.

## ACKNOWLEDGMENTS

We thank our colleagues from the NMC for numerous discussions and from the E665 and HERA Collaborations for providing us with their data. This research has been supported in part by the Polish State Committee for Scientific Research Grant No. 2 P302 062 04.

## REFERENCES


Abramowicz, H., 1995 (private communication).
Abramowicz, H., K. Charchuła, M. Krawczyk, A. Levy, and U. Maor, 1993, Int. J. Mod. Phys. A **8**, 1005.
Abramowicz, H., E. M. Levin, A. Levy, and U. Maor, 1991, Phys. Lett. B **269**, 465.
Abt, I., *et al.* (H1 Collaboration), 1993, Nucl. Phys. B **407**, 515.
Adams, M. R., *et al.* (E665 Collaboration), 1992, Phys. Rev. Lett. **68**, 3266.
Adams, M. R., *et al.* (E665 Collaboration), 1993, Phys. Lett. B **309**, 477.
Adams, M. R., *et al.* (E665 Collaboration), 1995a, Z. Phys. C **67**, 403.
Adams, M. R. *et al.* (E665 Collaboration), 1995b, Phys. Rev. Lett. **75**, 1466.
Ahmed, T., *et al.* (H1 Collaboration), 1993, Phys. Lett. B **299**, 374.
Alekhin, S. I., *et al.* (HERA and COMPAS Groups), 1987, ''Compilation of Cross Sections,'' CERN-HERA 87-01.
Altarelli, G., 1982, Phys. Rep. **81**, 1.
Altarelli, G., and G. Parisi, 1977, Nucl. Phys. B **126**, 298.
Amaudruz, P., *et al.* (NMC), 1992a, Phys. Lett. B **294**, 120.
Amaudruz, P., *et al.* (NMC), 1992b, Phys. Lett. B **295**, 159.
Amaudruz, P., *et al.* (NMC); 1992c, preprint CERN-PPE/92-124; Erratum Oct. 26th, 1992; Erratum April 19th, 1993.
Amaudruz, P., *et al.* (NMC), 1992d, Nucl. Phys. B **371**, 3.
Amaudruz, P., *et al.* (NMC), 1995, Nucl. Phys. B **441**, 3.
Arneodo, M., 1994, Phys. Rep. **240**, 301.
Arneodo, M., *et al.* (EMC NA28), 1990, Nucl. Phys. B **333**, 1.
Arneodo, M., *et al.* (NMC), 1993, Phys. Lett. B **309**, 222.
Arneodo, M., *et al.* (NMC), 1994, Phys. Rev. D **50**, R1.
Arneodo, M., *et al.* (NMC), 1995a, preprint CERN-PPE/95-138 (submitted to Physics. Lett. B).
Arneodo, M., *et al.* (NMC), 1995b, Nucl. Phys. B **441**, 12.
Arnold, R. G., *et al.* (SLAC E139), 1984, Phys. Rev. Lett. **52**, 727.
Aubert, J. J., *et al.* (EMC NA2), 1987, Nucl. Phys. B **293**, 740.
Badełek, B., D. Bardin, K. Kurek, and C. Scholz, 1995, Z. Phys. C **66**, 591.
Badełek, B., S. Bentvelsen, P. Kooijman, J. Kwieciński, H. Spiesberger, and W. von Schlippe 1993, J. Phys. G **19**, 1671.
Badełek, B., K. Charchuła, M. Krawczyk, and J. Kwieciński, 1992, Rev. Mod. Phys. **64**, 927.
Badełek, B., and J. Kwieciński, 1992, Phys. Lett. B **295**, 263.
Badełek, B., and J. Kwieciński, 1994, Phys. Rev. D **50**, R4.
Badełek, B., J. Kwieciński, and A. Staśto, 1996, Durham preprint DTP/96/16.
Balitskij, Ya. Ya., and L. N. Lipatov, 1978, Yad. Fiz. **28**, 1597 [Sov. J. Nucl. Phys. **28**, 822 (1978)].
Barone, V., M. Genovesse, N. N. Nikolae, E. Predazzi, and B. G. Zakharov, 1994, Phys. Lett. B **321**, 137.
Bauer, T. H., R. D. Spital, D. R. Yennie, and F. M. Pipkin, 1978, Rev. Mod. Phys. **50**, 261.
Benvenuti, A. C., *et al.* (BCDMS Collaboration), 1989, Phys. Lett. B **223**, 485.
Benvenuti, A. C., *et al.* (BCDMS Collaboration), 1990, Phys. Lett. B **237**, 592.
Bodek, A., and U. K. Yang, 1995, lecture delivered at the UK Phenomenology Workshop on HERA Physics, Durham, UK, September 1995 (to be published in J. Phys. G).
Brasse, F. W., W. Flanger, J. Gyler, S. P. Goel, R. Haidan, M. Merkowitz, and H. Wriedt, 1976, Nucl. Phys. B **110**, 413.
Bronzan, J. B., and R. L. Sugar, 1978, Phys. Rev. D **17**, 585.
Brüll, A. (NMC), 1995, lecture delivered at the International Europhysics Conference on High-Energy Physics, Brussels, July 27–August 2, 1995 (to appear in the Proceedings).
Butterworth, J. M., and J. R. Forshaw, 1993, J. Phys. G **19**, 1657.
Capella, A., A. Kaidalov, C. Merino, and J. Trân Thanh Vân, 1994, Phys. Lett. B **337**, 358.
Carroll, T. (E665), 1995, lecture delivered at the International Europhysics Conference on High-Energy Physics, Brussels, July 27–August 2, 1995 (to appear in the Proceedings).
Catani, S., F. Fiorani, and G. Marchesini, 1990a, Phys. Lett. B **234**, 339.
Catani, S., F. Fiorani, and G. Marchesini, 1990b, Nucl. Phys. B **336**, 18.
Ciafaloni, M., 1988, Nucl. Phys. B **296**, 49.
Collins, P. D. B., 1977, *An Introduction to Regge Theory and High Energy Physics* (Cambridge University, Cambridge).
Derrick, M., *et al.* (ZEUS Collaboration), 1992, Phys. Lett. B **293**, 465.
Derrick, M., *et al.* (ZEUS Collaboration), 1993, Phys. Lett. B **316**, 412.
Derrick, M., *et al.* (ZEUS Collaboration), 1994, Z. Phys. C **63**, 391.
Dokshitzer, Yu. L., V. A. Khoze, A. H. Mueller, and S. I. Troyan, 1991, *Basics of Perturbative QCD* (Editions Frontiéres, Gif-sur-Yvette, France).
Donnachie, A., and P. V. Landshoff, 1984, Nucl. Phys. B **244**, 322.
Donnachie, A., and P. V. Landshoff, 1992, Phys. Lett. B **296**, 227.
Donnachie, A., and P. V. Landshoff, 1994, Z. Phys. C **61**, 139.
Dyring, A. (NMC), 1994, *QCD and High Energy Hadronic Interactions*, Proceedings of the XXIX Rencontre de Morionod, March 19–26, 1994, Méribel les Allues, Savoie, France, edited by J. Trân Thanh Vân (Editions Frontiéres, Gif-sur-Yvette, France), p. 199.
Dyring, A., 1995, Ph.D., Uppsala University.
Eisele, F., 1995, lecture delivered at the International Europhysics Conference on High Energy Physics, Brussels, July 27–August 2, 1995 (to appear in the Proceedings).
Forshaw, J. R., 1992, Phys. Lett. B **285**, 354.
Forshaw, J. R., and J. K. Storrow, 1991, Phys. Lett. B **268**, 116; **276**, 565(E).
Forshaw, J. R., and J. K. Storrow, 1994, Phys. Lett. B **321**, 151.
Ghandi, R., I. Sarcevic, A. Burrows, L. Durand, and H. Pi, 1990, Phys. Rev. D **42**, 263.
Glauber, R. J., 1959, in *Lectures in Theoretical Physics*, edited by W. E. Brittin and L. G. Dunham (Wiley Interscience, New York), Vol. I, p. 315.
Glück, M., and E. Reya, 1993, Dortmund preprint DO-TH 93/27.
Glück, M., E. Reya, and A. Vogt, 1992, Z. Phys. C **53**, 127.
Glück, M., E. Reya, and A. Vogt, 1993, Phys. Lett. B **306**, 391.
Glück, M., E. Reya, and A. Vogt, 1995, Z. Phys. C **67**, 433.
Gordon, B. A., *et al.* (CHIO Collaboration), 1979, Phys. Rev. D **20**, 2645.
Grammer, G., Jr., and J. D. Sullivan, 1978, in *Electromagnetic Interactions of Hadrons*, edited by A. Donnachie and S. Shaw (Plenum, New York), Vol. 2.
Granier, T. (NMC), 1994, in *QCD and High Energy Hadronic Interactions*, Proceedings of the XXIX Rencontre de Mori-

ond, March 19–26 1994, Méribel les Allues, Savoie, France, edited by J. Trân Thanh Vân (Editions Frontiéres, Gif-sur-Yvette, France), p. 205.
Gribov, L. V., E. M. Levin, and M. G. Ryskin, 1983, Phys. Rep. **100**, 1.
Halzen, F., and A. D. Martin, 1984, *Quarks and Leptons: An Introductory Course in Modern Particle Physics* (Wiley, New York).
Honjo, K., L. Durand, R. Ghandi, H. Pi, and I. Sarcevic, 1993, Phys. Rev. D **48**, 1048.
Jaroszewicz, T., 1980, Acta. Phys. Pol. B **11**, 965.
Kopeliovich, B. Z., and P. J. Marage, 1993, J. Mod. Phys. A **8**, 1513.
Kotwal, A. V. (E665 Collaboration), 1994, lecture delivered at the VIth Rencontre de Blois, June 1994, Blois, France.
Kotwal, A. V., 1995, Ph.D. thesis, Harvard University.
Kotwal, A. V., *et al.* (E665 Collaboration), 1995, preprint FERMILAB-CONF-95-46 (to appear in *QCD and High Energy Hadronic Interactions*, Proceedings of the XXX Rencontre de Moriond, March 1995, Les Arcs, France).
Kuraev, E. A., L. N. Lipatov, and V. S. Fadin, 1977, Zh. Éksp. Teor. Fiz. **72**, 373 [Sov. Phys.-JETP **45**, 199 (1977)].
Kwieciński, J., 1993, J. Phys. G **19**, 1443.
Kwieciński, J., 1994, in *Substructures of Matter as Revealed with Electroweak Probes*, Proceedings of the 32nd Schladming Winter School, Lecture Notes in Physics, No. 426, edited by L. Mathelisch and W. Plessas (Springer, Berlin), 215.
Kwieciński, J., and B. Badełek, 1989, Z. Phys. C **43**, 251.
Landshoff, P. V., J. C. Polkinghorne, and K. D. Short, 1971, Nucl. Phys. B **28**, 225.
Levin, E. M., and M. G. Ryskin, 1990, Nucl. Phys. B, Proc. Suppl. **18C**, 92.
Levy, A., 1993, J. Phys. G **19**, 1489.
Levy, A., 1995a, lecture delivered at the International Europhysics Conference on High Energy Physics, Brussels, July 27–August 2, 1995 (to appear in the Proceedings).
Levy, A., 1995b, lecture delivered at the UK Phenomenology Workshop on HERA Physics, Durham, UK, September, 1995 (to be published in J. Phys. G).
Lipatov, L. N., 1989, in *Perturbative QCD*, edited by A. H. Mueller (World Scientific, Singapore), p. 411.
Martin, A. D., 1994, Acta. Phys. Pol. B **25**, 265.
Martin, A. D., W. J. Stirling, and R. G. Roberts, 1993a, Phys. Rev. D **47**, 145.
Martin, A. D., W. J. Stirling, and R. G. Roberts, 1993b, Phys. Rev. B **306**, 145.
Martin, A. D., W. J. Stirling, and R. G. Roberts, 1994, Phys. Rev. D **50**, 6734.
Martin, A. D., W. J. Stirling, and R. G. Roberts, 1995, Phys. Rev. D **51**, 4756.
Melnitchouk, W., and A. W. Thomas, 1993a, Phys. Rev. D **47**, 3783.
Melnitchouk, W., and A. W. Thomas, 1993b, Phys. Lett. B **317**, 437.
Merino, C., 1994, in *QCD and High Energy Hadronic Interactions*, Proceedings of the XXIX Rencontre de Moriond, March 19–26, 1994, Méribel les Allues, Savoie, France, edited by J. Trân Thanh Vân (Editions Frontiéres, Gif-sur-Yvette, France), p. 271.
Mestayer, M. D., 1978, Ph.D. thesis, Stanford University, SLAC-Report-214.
Mücklich, A. (NMC), 1995, Proceedings of the Workshop on Deep Inelastic Scattering and QCD, April 1995, Paris, France, edited by J.-F. Laporte and Y. Sirois, p. 489.
Müller, K. (H1 Collaboration), 1994, in *QCD and High Energy Hadronic Interactions*, Proceedings of the XXIX Rencontre de Moriond, 1994, Méribel les Allues, Savoie, France, edited by J. Trân Thanh Vân (Editions Frontiéres, Gif-sur-Yvette, France), p. 163.
Reya, E., 1981, Phys. Rep. **69**, 195.
Roberts, R. G., 1990, *The Structure of the Proton: Deep Inelastic Scattering* (Cambridge University, Cambridge).
Roberts, R. G., 1992 (private communication).
Roco, M. (ZEUS Collaboration), 1994, in *QCD and High Energy Hadronic Interactions*, Proceedings of the XXIX Rencontre de Moriond, 1994, Méribel les Allues, Savoie France, edited by J. Trân Thanh Vân (Editions Frontiéres, Gif-sur-Yvette, France), p. 157.
Rujula de, A., H. Georgi, and H. D. Politzer, 1977, Ann. Phys. **103**, 315.
Schuler, G. A., and T. Sjöstrand, 1993, Nucl. Phys. B **407**, 425.
Seitz, R., and A. Witzmann (NMC), 1993, Proceedings of the XXVIII Rencontre de Moriond, in *QCD and High Energy Hadronic Interactions*, Les Arcs, Savoie, France, March 20–27 1993, edited by J. Trân Thanh Vân (Editions Frontiéres, Gif-sur-Yvette, France).
Storrow, J. K., 1993, J. Phys. G **19**, 1641.
Virchaux, M., and A. Milsztajn, 1992, Phys. Lett. B **274**, 221.
Vogt, A., 1995 (private communication).
Whitlow, L. W., E. M. Riordan, S. Dasu, S. Rock, and A. Bodek (SLAC), 1992, Phys. Lett. B **282**, 475.
Whitlow, L. W., S. Rock, A. Bodek, S. Dasu, and E. M. Riordan, 1990, Phys. Lett. B **250**, 193.
Witzmann, A. (NMC), 1995, lecture delivered at the International Europhysics Conference on High Energy Physics, Brussels, July 27–August 2, 1995 (to appear in the Proceedings and to be submitted to Nucl. Phys. B).
Yang, U., 1995, lecture delivered at the UK Phenomenology Workshop on HERA Physics, Durham, UK, September, 1995 (to appear in J. Phys. G).
Zoller, V. R., 1992a, Z. Phys. C **54**, 425.
Zoller, V. R., 1992b, Phys. Rev. Lett. B **279**, 145.